Peer-reviewed version available at *Geosciences* **2018**, *8*, 128; doi:10.3390/geosciences8040128

Article

Basin Resonance and Seismic Hazard in Jakarta, Indonesia

Athanasius Cipta [1], Phil Cummins [2], Masyhur Irsyam [3], Sri Hidayati [4]

[1] Affiliation 1; athanasius.cipta@anu.edu.au; Research School of Earth Sciences, Australian National University; Badan Geologi
[2] Affiliation 2; phil.cummins@anu.edu.au; Research School of Earth Sciences, Australian National University; GeoScience Australia
[3] Affiliation 3; masyhur.irsyam@yahoo.com; Civil Engineering Dept. Institut Teknologi Bandung, Jl. Ganesha No. 10, Bandung
[4] Affiliation 4; ichi@vsi.esdm.go.id; Badan Geologi
* Correspondence: athanasius.cipta@anu.edu.au

Abstract: We use earthquake ground motion modelling via Ground Motion Prediction Equations (GMPEs) and numerical simulation of seismic waves to consider the effects of site amplification and basin resonance in Jakarta, the capital city of Indonesia. While spectral accelerations at short periods are sensitive to near-surface conditions (i.e., Vs30), our results suggest that, for basins as deep as Jakarta's, available GMPEs cannot be relied upon to accurately estimate the effect of basin depth on ground motions at long periods (>1 s). Amplitudes at such long periods are influenced by entrapment of seismic waves in the basin, resulting in longer duration of strong ground motion, and interference between incoming and reflected waves as well as focusing at basin edges may amplify seismic waves. In order to simulate such phenomena in detail, a basin model derived from a previous study is used as a computational domain for deterministic earthquake scenario modeling in a 2-dimensional cross-section. A M_w 9.0 megathrust, a M_w 6.5 crustal thrust and a M_w 7.0 instraslab earthquake are chosen as scenario events that pose credible threats to Jakarta, and the interactions with the basin of seismic waves generated by these events were simulated. The highest PGV amplifications are recorded at sites near the middle of the basin and near its southern edge, with maximum amplifications of PGV in the horizontal component of 200% for the crustal, 600% for the megathrust and 335% for the deep intraslab earthquake scenario, respectively. We find that the levels of response spectral acceleration fall below those of the 2012 Indonesian building Codes's design response spectrum for short periods (< 1 s), but closely approach or may even exceed these levels for longer periods.

Keywords: seismic hazard; openquake; GMPE; basin-induced amplification; SPECFEM2D

1. Introduction

An assessment of ground shaking due to potential earthquake scenarios for a metropolitan area is of great importance for risk mitigation. As the world's 4th largest urban agglomeration (*Brinkhoff* [9]) located in a tectonically active region, greater Jakarta, Indonesia, is a potential hotspot for global earthquake risk. One important factor to consider in assessing this risk is the seismic response of the Jakarta Basin. Basin structure can have a profound influence on seismic ground motion, and various methods have been used to take this into account in seismic hazard studies. These methods can be simply divided into 2 main approaches. The first approach uses depth Z_{V_S} to a reference shear-wave velocity, V_S, taken to represent seismic basement, as a parameter in Ground Motion Prediction Equations (GMPEs, see, e.g. *Chiou & Youngs* [13] and *Campbell & Bozorgnia* [11]). Because GMPEs are independent of source-receiver path, this approach allows basin effects to be taken into account in most implementations of Probabilistic Seismic Hazard Analysis (PSHA). The second approach uses numerical modelling of seismic waves and depends on the source-site path (see, e.g.

Peer-reviewed version available at Geosciences 2018, 8, 128; doi:10.3390/geosciences8040128

Graves [20], *Bard & Bouchon* [7] and *Furumura and Chen* [16]). This approach offers a much more complete treatment of the ground motion, but because of its source-site path dependence it cannot be effectively used in PSHA. In this study we consider the efficacy of both approaches in assessing seismic hazard in Jakarta, using a recently developed model of the Jakarta Basin (*Cipta, et al.* [12]).

Recent Ground Motion Prediction Equations (GMPEs) incorporate sedimentary basin effects by using the depth at which shear-wave velocity reaches 1.0 km/s, denoted $Z_{1.0}$ (e.g. *Chiou & Youngs* [13] and *Abrahamson et al.* [3]), or 2.5 km/s, denoted $Z_{2.5}$, to parametrize basin depth. The latter is thought to be a better description of basin depth (*Marafi et al.* [29]). In this study, the GMPEs from *Chiou & Youngs* [13] and *Campbell & Bozorgnia* [11] are used to compute ground motions triggered by a crustal earthquake, while for the megathrust *Abrahamson et al.* [3] is used, and for intraslab events *Abrahamson et al.* [3] (intraslab) is used. In this chapter, these GMPEs are referred as CY2014, CB2014, AEA2015 and AEA2015S, respectively. In all cases where a GMPE is used with depth to a particular reference velocity Z_{V_S}, that depth is determined from the Jakarta Basin model of *Cipta, et al.* [12], which is based on a Horizontal-to-Vertical Spectral Ratio (HVSR) analysis of ambient seismic noise.

The analysis of *Cipta, et al.* [12] also provides the model for the geometry of the Jakarta Basin that we use to simulate 2D seismic wave propagation along a NS cross section of the Jakarta Basin. Long period ground motion modeling was carried out by means of the SPECFEM2D software (http://geodynamics.org/cig/software/specfem2d/; *Komatitsch & Vilotte* [27]), which uses the spectral element method. These simulations are conducted to evaluate the effect of the Jakarta basin structure on long period ($\geq$1 s) ground-shaking in the city of Jakarta. Scenario modeling includes a megathrust, a medium-depth intraslab and shallow crustal earthquakes. The main objective of this paper is to analyse the effect of the deep sedimentary basin on amplification of long period ground motion in the city of Jakarta. Long duration ground shaking is expected to build up due to seismic wave entrapment inside the basin (*Graves* [20]) and the conversion of incident shear waves at the basin edge (*Bard & Bouchon* [7]).

The deep Jakarta basin is filled with alluvial fan and alluvium deposited continuously during the early Quaternary to the present day. Rapid subsidence of Jakarta soil due to water extraction – up to 26 cm per year (*Abidin et al.* [2], *Ng et al.* [36]) shows the high extent of water saturation of sediment fill. Underneath these Quaternary sediments lie volcaniclastic deposits of Pliocene-Pleistocene age that are mainly composed of tuff and locally tuffaceous breccia, lava and lahar. Volcanic material has ben shown to strongly amplify seismic ground motion – as high as 50 times compared to bedrock sites – in Mexico City during the event of 1985 Michoacán Earthquake (*Cruz-Atienza et al.* [14]). In Jakarta, a combination of volcanic, alluvial fan and alluvium deposits as thick as 300-1400 m overlie Tertiary bedrock. By numerical modelling of multiple earthquake scenarios, we can assess the variability of ground motion and amplification effects caused by the combination of basin geometry and soft sediment with the different earthquake scenarios.

Since the basin model of *Cipta, et al.* [12] is confined to the city limits of Jakarta, a paleo-topographic approach is used to identify the basin edges and extend the basin model derived from the HVSR method. This final basin model will be used as the computational domain for the SPECFEM2D code (*http://geodynamics.org/cig/software/specfem2d/*; *Komatitsch & Vilotte* [27]). In this study, waves originating from a megathrust event (M_w 9.0) propagate from 1002 source points through 5-layer domain model. The other scenarios, a shallow M_w 6.5 crustal and a medium-depth M_w 7.0 intraslab earthquake, use a smaller number of source points and elements.

2. Tectonic Setting of Jakarta and Surroundings

Java island, where Jakarta is located, is part of the Sunda Arc that extends from the Andaman Sea in the northwest to the Banda Sea in the east. The Australian Plate is moving northward at a rate of 67 (*Simons et al.* [46]) to 70 (*Hall* [21]) mm/yr and subducting beneath the Eurasian Plate. *Pusgen* [40] estimated that the Sunda Strait and West-Central Java segments of the Sunda Subduction Zone can accommodate earthquakes as large as Mw 8.7. These are the closest segments to Jakarta and located

Peer-reviewed version available at *Geosciences* **2018**, *8*, 128; doi:10.3390/geosciences8040128

about 250 km from the city to the south. In the last decade, the West-Central segment produced 2 destructive earthquakes, namely the Mw 7.6 Pangandaran (2006) and the Mw 7.0 Tasikmalaya (2009) Earthquakes *Pusgen* [40].

The tectonics and seismicity of Jakarta and adjacent areas is highly influenced by the the convergence of the Australian Plate toward the Eurasian Plate (Figure 1). Apart from producing megathrust earthquakes, the northward motion of the Australian Plate is also responsible for earthquake activity on shallow crustal faults, some of which are located near Jakarta such as the Cimandiri, Lembang and Baribis Faults. The Cimandiri Fault shows a dominant strike-slip movement with rake angle less than 15° and dip larger than 70° (*Dardji et al.* [15]). The same author also observed high-angle reverse movement, and argued that permutation between strike-slip and dip-slip systems may happen over relatively intervals along the strike of an active fault. Despite a disagreement regarding sense of movement, *Dardji et al.* [15], *Abidin et al.* [1], *Supartoyo et al.* [47], *Marliyani & Arrowsmith* [30] and *Handayani et al.* [22], using paleostress, GPS, morphometry, geomorphology and audio-magnetotelluric methods, respectively, conclude that the Cimandiri Fault is active and its segmentation limits the maximum magnitude of potential earthquakes.

The 24 km length of the Lembang Fault with a slip rate of 2.0 mm/yr is thought capable of producing a Mw 6.8 earthquake (*Pusgen* [40]). An earlier study by *Meilano et al.* [31] indicates a larger slip-rate (6 mm/yr) with fault locking at 3-15 km and this study also observed shallow creep at rate of 6 mm/yr. During 2009-2015, there were 4 earthquakes recorded along the Lembang Fault, three of which showed left-lateral faulting, and an earthquake located at the eastern edge of the fault showed oblique slip with a normal-dominant movement (*Pusgen* [40]).

The Baribis or Baribis-Kendeng Fault has been proposed as a major thrust and fold structure extending all the way across Java from the Sunda Strait in the west to beyond East Java in the east, and it is suggested that some segments are still active (*Simandjuntak & Barber* [45]). The strike-slip Cimandiri and Citanduy Faults cut across the Baribis-Kendeng Thrust near the border of West-Central Java and therefore it is not clear whether this is one single structure or is divided into the Baribis Thrust in the west and the Kendeng Thrust in the east. *Koulali et al.* [28] suggest that the Baribis Thrust is accommodating convergence between Java and the Sunda Block at about 5 mm/yr, while *Pusgen* [40] show the the Baribis-Kendeng Thrust as a highly segmented system of faults starting from Subang in the west (north of the Lembang Fault) to Surabaya in the east. Each segment can accommodate earthquakes in the magnitude range Mw 6.0 - Mw 6.5.

3. The Jakarta Basin

Earthquake-induced resonance is a phenomenon that occurs in deep sedimentary basins, as seen in Mexico City (*Cruz-Atienza et al.* [14], *Rial et al.* [42]) and Kathmandu (*Galetzka et al.* [17]) due to the 1985 Michoacán and 2015 Nepal earthquakes, respectively. Greater Jakarta (including Jakarta as well as the adjacent cities of Bekasi, Bogor, Depok, Tangerang and Tangerang Selatan) is the world's 4th largest urban agglomeration with a population of 28.9 million (*Brinkhoff* [9]), and has experienced destructive earthquakes in 1699 (*Nata & Witsen* [35]), 1780 (*Albini et al.* [4]) and 1834 (*Musson* [34]). Jakarta's high population, together with many tall buildings (67 $\geq$150 m in height, see *https://skyscrapercenter.com/city/jakarta*) and history of earthquake occurrence can be a deadly combination if seismic hazard not adequately addressed.

A model of the seismic velocity structure of the Jakarta Basin was constructed by *Cipta, et al.* [12] using analysis of Horizontal-to-Vertical Spectral Ratios (HVSR) of ambient seismic noise (Figure 2), but this model does not extend to the basin edges. The sediment deposits along the city border are thick, from about 200 m in the south, 800 m in the west and more than 1000 m in the east. Because the model does not include the basin edges, it is necessary to extend the model beyond Jakarta itself to estimated plausible margins of the basin, which are presumed to be the axes of low angle folds that will appear as topographic highs. For this purpose, geological data namely, the lateral distribution of lithology, drainage pattern and topographic information was utilized. A simple method to reconstruct

Peer-reviewed version available at *Geosciences* **2018**, *8*, 128; doi:10.3390/geosciences8040128

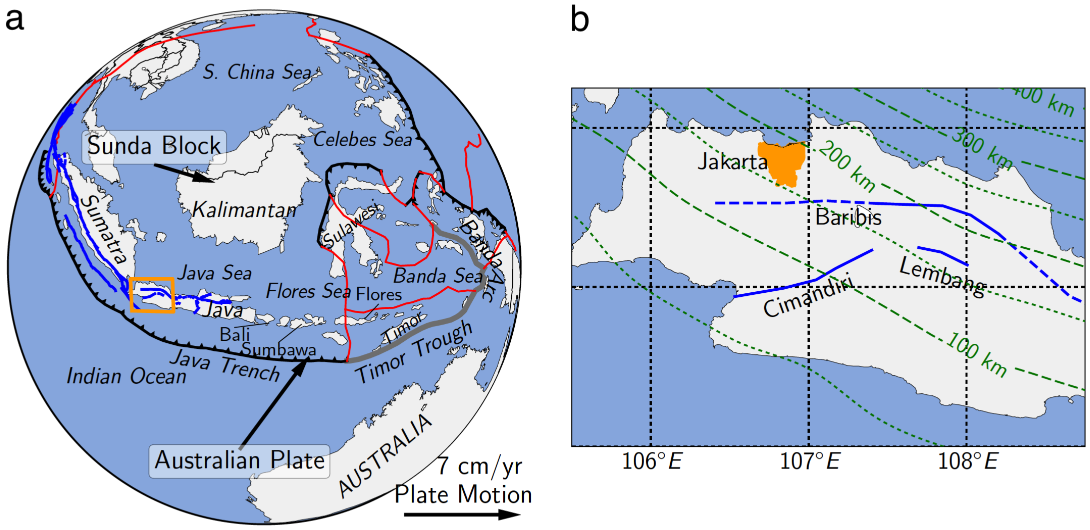

Figure 1. (**a**) Simplified tectonic setting of the Indonesian region and (**b**) western Java, with more detail of the inset area indicated in (**a**). The study area is the orange shaded area in (**b**). Motion of the Australian Plate at a rate of 7 cm a year toward the Eurasian Plate is indicated by a black arrow. Major faults are indicated by blue lines, while black toothed, red and green dashed lines denoted subduction, microcontinent boundaries, and Benioff countours, respectively. The blue dashed-line indicates the continuation of the Baribis fault to the west and east as mentioned in *Simandjuntak & Barber* [45].

the paleo-topography called the arc-method is used (for detail see e.g. *Allmendinger* [5]). By comparing geological data and sediment thickness as presented in Figure 2, it is a reasonable guess to interpret the basement of the basin as the upper Parigi formation deposited in the Late Miocene. To construct a paleotopography, i.e. a topography before the more recent Cibuluh formation was deposited, we need to plot the strike and dip of the Parigi formation layering in a 2D cross-section.

The topographic map shows that Jakarta in particular and the north coast of West Java in general is an area of gentle slope (slope 1-10 %). The morphology and surface lithology of this area is well illustrated in its drainage pattern, an excellent example of a dendritic drainage pattern characteristic of gentle topography with homogeneous lithology. Careful analysis of the drainage pattern discloses the faint topographic highs to the west and east of the city. Most of the tributaries of the Cisadane River (1 In Figure 3) flow only from the west, while further to the west the Cimanceuri River (4 in Figure 3) flows from the south, veers westward then flows northward. These 2 rivers encircle a topographic high that can be identified with the western rim of the Jakarta basin. The geological map shows that near the Cimanceuri River (4 In Figure 3) the lithology is changing from aluvial fan Qav to QT tuff (north) and Oligocene-Miocene formations (south). This changing lithology confirms the hypothesis that the Cimanceuri River lies at the western rim of the Jakarta basin, in the slightly elevated land that is known as the Tangerang High.

The Kali Bekasi River (3 in Figure 3) to the east of the city receives water intake mostly from the east, and further to the east the Citarum River (5 in Figure 3) flows from the south, turns to the east and circles back to the west, eventually flowing into the Kali Bekasi River and the Java Sea. This drainage pattern is indicative of a topographic high just east of the Kali Bekasi River, known as the Rengasdengklok High. The Kali Bekasi River also marks the boundary between two alluvial fan bodies, alluvial fan Qav to the west of the Kali Bekasi River, and alluvial fan Qav/Qos to the east of the river. The changing lithology and topographic high to the east suggest that the eastern rim of the basin is situated around the Kali Bekasi River.

Oil prospecting studies using the seismic reflection method have succesfully recognized five principal oil reservoir groups within the North West-Java Basin. These oil caps are **(1)** Eocene–Oligocene

Peer-reviewed version available at Geosciences 2018, 8, 128; doi:10.3390/geosciences8040128

fractured volcanics (Jatibarang Volcanics), **(2)** Oligocene–Lower Miocene deltaic sandstones (Talang Akar Formation), **(3)** Lower Miocene reefs (Baturaja Formation), **(4)** Lower–Middle Miocene sandstones (Upper Cibulakan Formation), and **(5)** Middle-Upper Miocene carbonates (Parigi Limestones and Upper Cibulakan Formation) (*Kingston* [25]). On the top of these reservoirs, the Parigi, Cibuluh and Quaternary formations were deposited successively, with a hiatus due to decreasing sea level separating these formations. From these data, it can be inferred that the Jakarta Basin, also known as the Ciputat Basin, is part of the North West-Java Basin in which the basement is composed of carbonates of the the upper Parigi formation deposited in the Middle-Upper Miocene (see Figure 6 in *Putra et al.* [41]).

Since the HVSR-derived model provided by *Cipta, et al.* [12] covers only about 80% of the city, much less than the Ciputat Basin, we need to extend the coverage area to the basin's rims in order to simulate wave propagation in a more realistic basin geometry that minimizes any artefacts associated with an artificially abrupt basin edge. The arc method, also known as the Busk method (named after H. G. Busk and nicely explained in *Allmendinger* [5]), is used to reconstruct the carbonates of the Parigi Formation, so that the basin basement extends outside the area in which it is inferred from the HVSR measurements. In using the arc method, it is assumed that the stratigraphy of the Parigi formation has not been strongly affected by erosion. The final basin model, which is the composite of the HVSR-derived model (covering the city) and that derived using the arc method (covering outside the city to the basin's rim) is presented in Figure 4.

4. Material and Methods

4.1. Ground Motion Prediction Equations (GMPEs)

A GMPE is a generic term for a mathematical relationship between a statistical estimate of expected ground motion, and earthquake magnitude and some measure of distance to the earthquake fault rupture. GMPEs can supply a probability density function of ground motion values for a given earthquake scenario. These equations provide probabilistic descriptions of the level of ground shaking as a function of the earthquake parameters, accounting for path and site effects. Some New Generation Attenuation (NGA) functions take into account independent estimator variables such as earthquake magnitude (f_{mag}), geometric attenuation (f_{dis}), style of faulting(f_{flt}), hanging-wall geometry (f_{hng}), shallow site response (f_{site}), basin response (f_{sed}), hypocentral depth (f_{hyp}), rupture dip (f_{dip}), and (apparent) anelastic attenuation (f_{atn}) (*Campbell & Bozorgnia* [10]). They model a ground motion parameter Y, which could represent Peak Ground Acceleration (PGA), Peak Ground Velocity (PGV) or spectral acceleration (SA) at specific periods as:

$$lnY = f_{mag} + f_{dis} + f_{flt} + f_{hng} + f_{site} + f_{sed} + f_{hyp} + f_{dip} + f_{atn} \tag{1}$$

Out of these parameters, we are interested in investigating the f_{sed} parameter, which is intended to parametrize basin depth. The preliminary ground motion simulations are readily performed as the selected NGA GMPEs (CY2014 and CB2014) are incorporated in OpenQuake, a software platform developed by the Global Earthquake Model (GEM) Foundation for seismic hazard and risk calculations. The source code for this software is openly downloadable from a public repository www.github.com/gem, and operates on operating systems such as Linux, MacOS and Windows (*GEM* [19]).

The three GMPEs mentioned above require site parameters that use V_S30 as a proxy for near-surface geology (soil) classification, and $Z_{1.0}$ or $Z_{2.5}$ to describe basin depth ($Z_{1.0}$ is the depth to a V_S of 1 km/s, while $Z_{2.5}$ is depth to 2.5 km/s). Using data from Japan and California, *Chiou & Youngs* [13] provide empirical equations relating V_S30 and $Z_{1.0}$ and *Campbell & Bozorgnia* [10] provide empirical equations to estimate $Z_{2.5}$. To asses whether the velocity structure of the Jakarta Basin covers a similar parameter range to those in California and Japan that are used for these GMPEs, we plotted

Peer-reviewed version available at Geosciences 2018, 8, 128; doi:10.3390/geosciences8040128

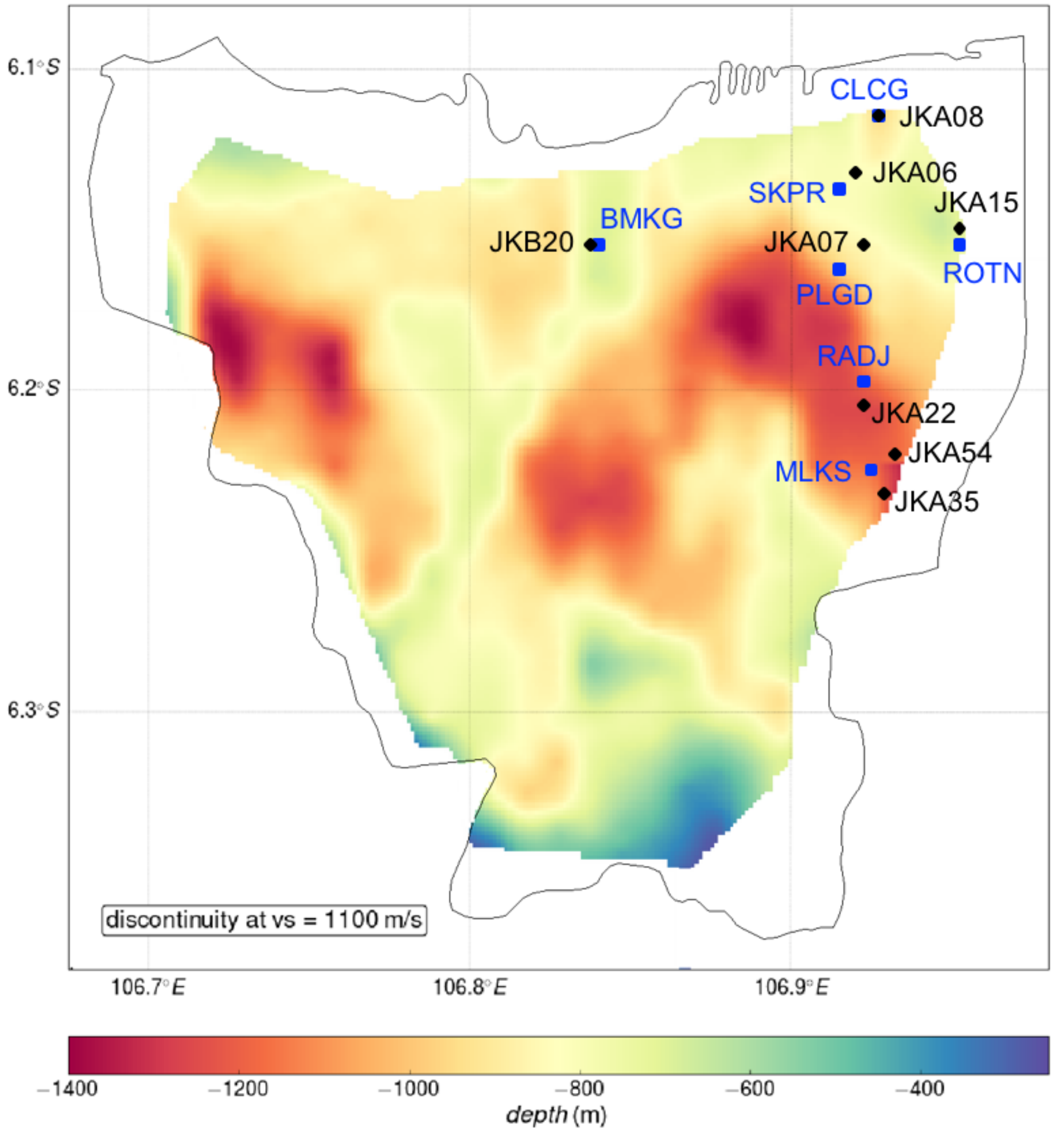

Figure 2. Considering shear-wave velocity V_S=1300 m/s as the basin bottom, we can map the geometry of the basin. Inside the city, the basin depth ranges from 300 m in the southeast to more than 1300 m in the northwest and northeast. The labelled black diamonds and blue squares are HVSR and SPAC co-located stations.

Peer-reviewed version available at *Geosciences* **2018**, *8*, 128; doi:10.3390/geosciences8040128

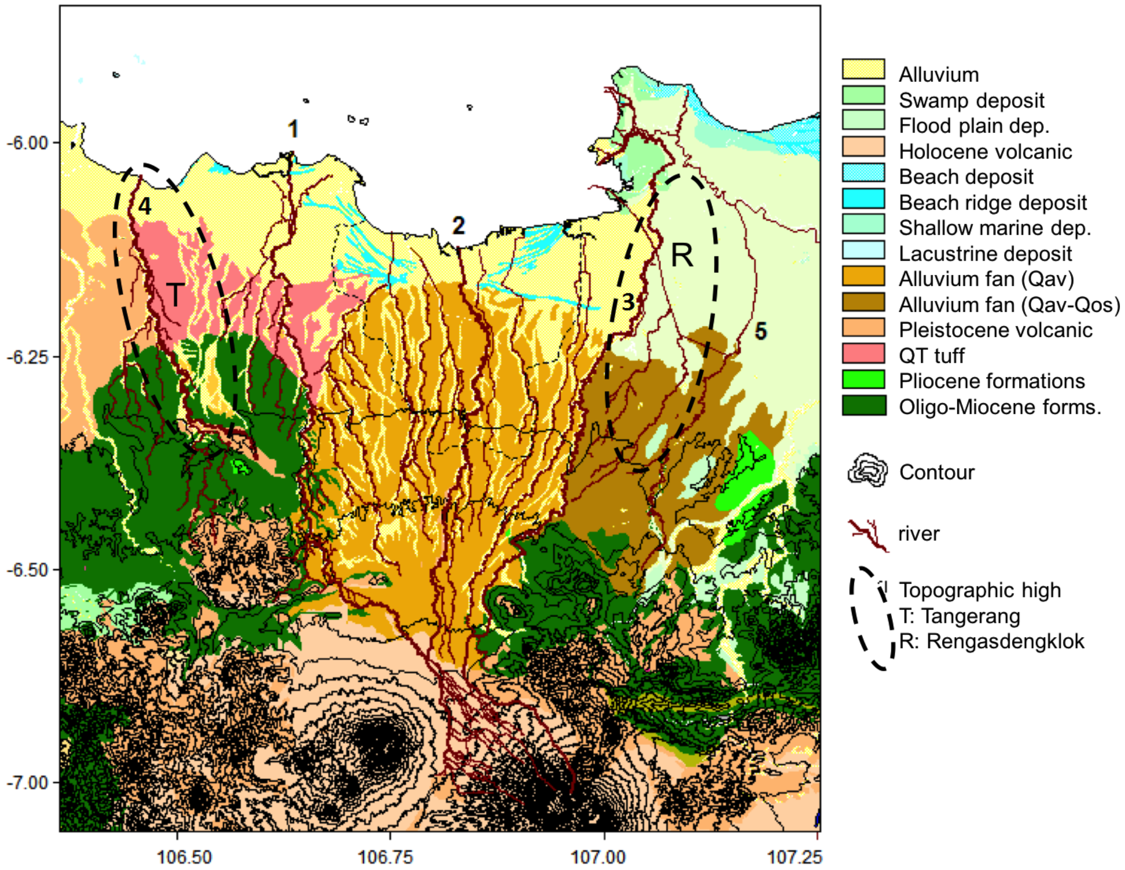

Figure 3. Contour lines and drainage patterns overlaid on a map of surface geology show the funnel-shaped basin, bounded by the Cisadane (1) and Kali Bekasi (3) Rivers in the west and east, respectively. Mountains from which the Cisadane (1), Ciliwung (2) and Kali Bekasi (3) Rivers sprout form the narrow base of a funnel-shaped topographic low with Jakarta Bay at its mouth. The Cimanceuri River is labeled as (4). The SN Line is the cross-section of domain area used in simulation.

Peer-reviewed version available at Geosciences 2018, 8, 128; doi:10.3390/geosciences8040128

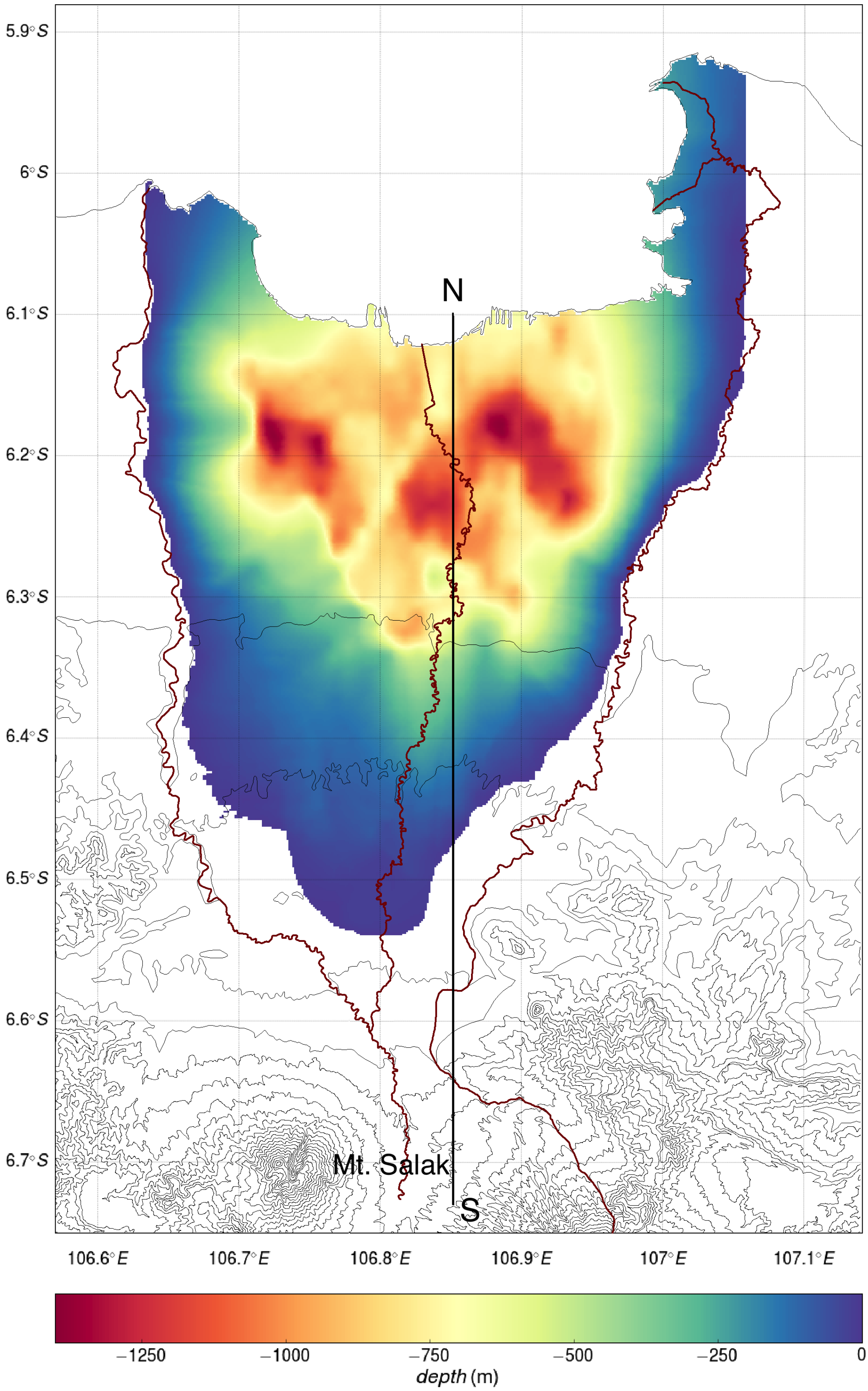

Figure 4. The extended basin model presented here merges the basin model derived from the HVSR technique that covered only the city of Jakarta with the result of the arc (Busk) method that considered geological data to estimate the basin edges.

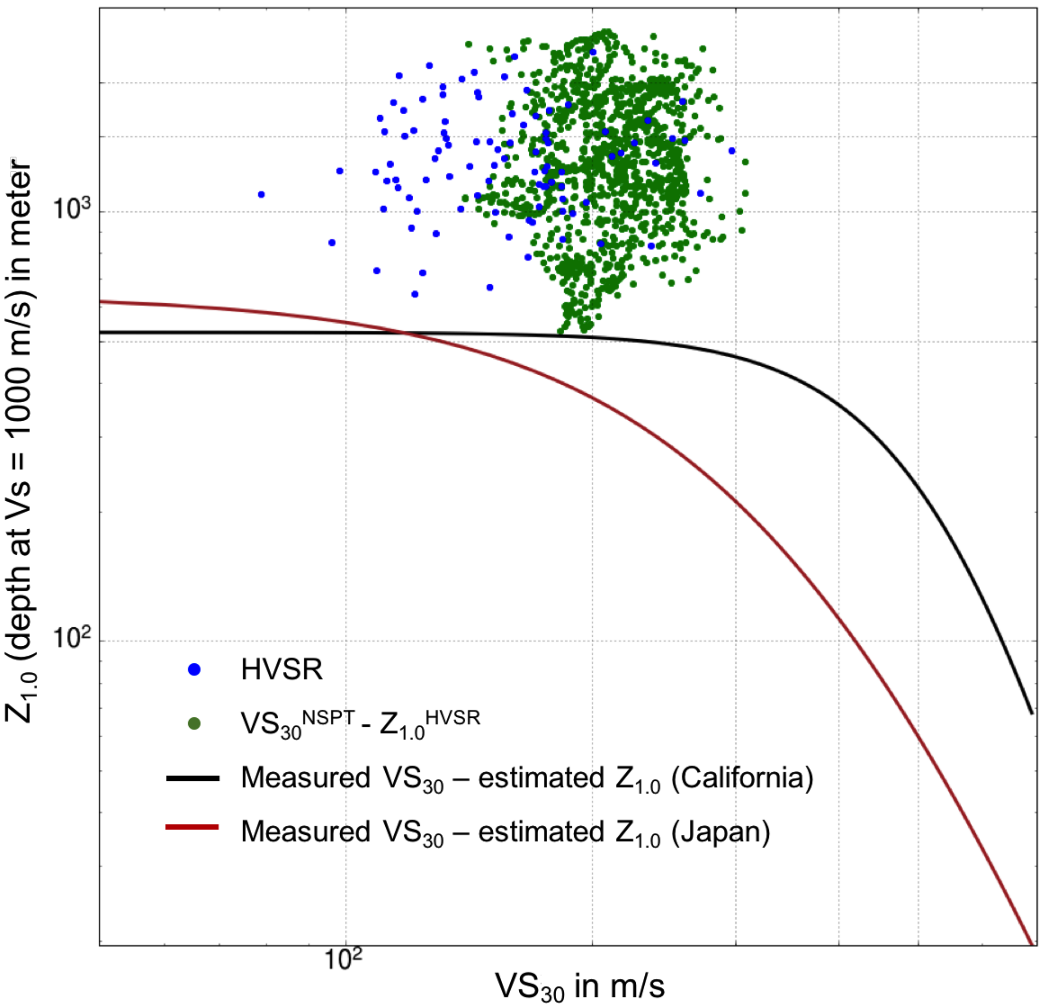

Figure 5. Plot of V_S30 against $Z_{1.0}$ and curves showing estimated $Z_{1.0}$ as a function of measured and computed V_S30 derived by *Chiou & Youngs* [13] from data taken in California (black line) and Japan (brown line). The blue and green dots are plots of $Z_{1.0}$ from the *Cipta, et al.* [12] model for the Jakarta Basin plotted against V_S30 taken from the same model and from the NSPT data of *Ridwan* [43], respectively.

the empirical equations of *Chiou & Youngs* [13] for $Z_{1.0}$ as a function of V_S30 against data from the *Cipta, et al.* [12] model for the Jakarta Basin, where $Z_{1.0}$ is taken directly from the model and V_S30 is either taken from the *Cipta, et al.* [12] model or the NSPT data of *Ridwan* [43]. Regardless of which estimate of V_S30 is used, Figure 5 shows that depths for the Jakarta Basin are always much greater than the $Z_{1.0}$ calculated from the *Chiou & Youngs* [13] empirical relations, either for California or Japan. Thus, the Jakarta Basin would appear to be much deeper than those for which the deep sediment adjustments to the *Chiou & Youngs* [13] GMPE were developed, and the same is almost certainly true for the *Campbell & Bozorgnia* [10], since it was based on a similar dataset. As a consequence, caution should be exercised when using these GMPEs to account for the effect of deep sediments in Jakarta.

4.2. Numerical Simulation of Seismic Waves

Earthquake-generated ground shaking depends not only on the earthquake source parameters, but also on the medium in which seismic waves propagate, especially near surface and basin structure. In this study, seismic waves generated by synthetic ruptures on a crustal fault, the Java Megathrust, and an intraslab fault are simulated using SPECFEM2D. This software uses the Spectral Element

Peer-reviewed version available at Geosciences 2018, 8, 128; doi:10.3390/geosciences8040128

Method (SEM), which combines the flexibility of the finite element method (FEM) with the accuracy of high-order (trigonometric) element basis functions. SEM is very effective at achieving high accuracy even for realistic earth models, and is therefore applicable for a wide range of applications in seismology (*Komatitsch & Vilotte* [27]). This approach to scenario ground modelling is similar to that used by *Molnar et al.* [3233] to study seismic wave interaction with 3D structure of the Georgia Basin, British Columbia, Canada.

The seismic characteristics of the Jakarta Basin as obtained from the HVSR analysis will be represented in our 2D domain as a SN cross section over which the earthquake simulation takes place. This simulation aims to analyze the effect of basin geometry on seismic hazard. To avoid extremely small elements, the sediment inside the basin is taken to be a homogeneous medium overlying bedrock, which is part of a 3-layer lithosphere, with maximum domain area as large as 445 km in length by 150 km in depth (Figure 6). The shear-wave velocity both in the sediment-filled basin and bedrock are taken as averages from the corresponding depths of the HVSR model. Crustal P-wave velocity (V_P) outside the basin is taken to be 1.8 times V_S as indicated in *Cipta, et al.* [12].

Secondly, earthquake scenarios that each pose a credible risk to Jakarta are chosen by referring to *Nguyen et al.* [37], whose analysis of historical data and earthquake simulations identified 3 sources that may have severely affect Jakarta in the past: a large megathrust event, a shallow crustal event, and a medium-depth intraslab event. A scenario for each of these event types is considered in this study.

The surface geology in the area of interest, from older to younger deposits, is composed of Tertiary marine formations, Pliocene-Pleistocene volcanic rocks, alluvial fan and recent alluvium. Alluvial fan deposits are the main component filling the basin, overlaying the Tertiary-Quaternary volcanic rocks that are presumed to act as basement. It is also possible that Miocene marine deposits play a role as bedrock, especially in the northern part of the basin. Heterogeneities both in vertical and horizontal directions make it difficult to set the elastic properties of the basin, particularly since the very low V_S(<100 m/s) near the surface will require extremely small elements to model accurately. Instead of describing the detailed spatial variation of basin velocities, V_S is set to the average velocity in the basin resulting from inversion of HVSR ellipticity curves, 582m/s. Compressional-wave velocity (V_P) in the basin is set to 3-4 times V_S under the assumption that as a groundwater basin, the sediments filling Jakarta Basin are highly saturated, as also indicated by HVSR inversion that shows high (~ 4) V_P/V_S (*Cipta, et al.* [12]).

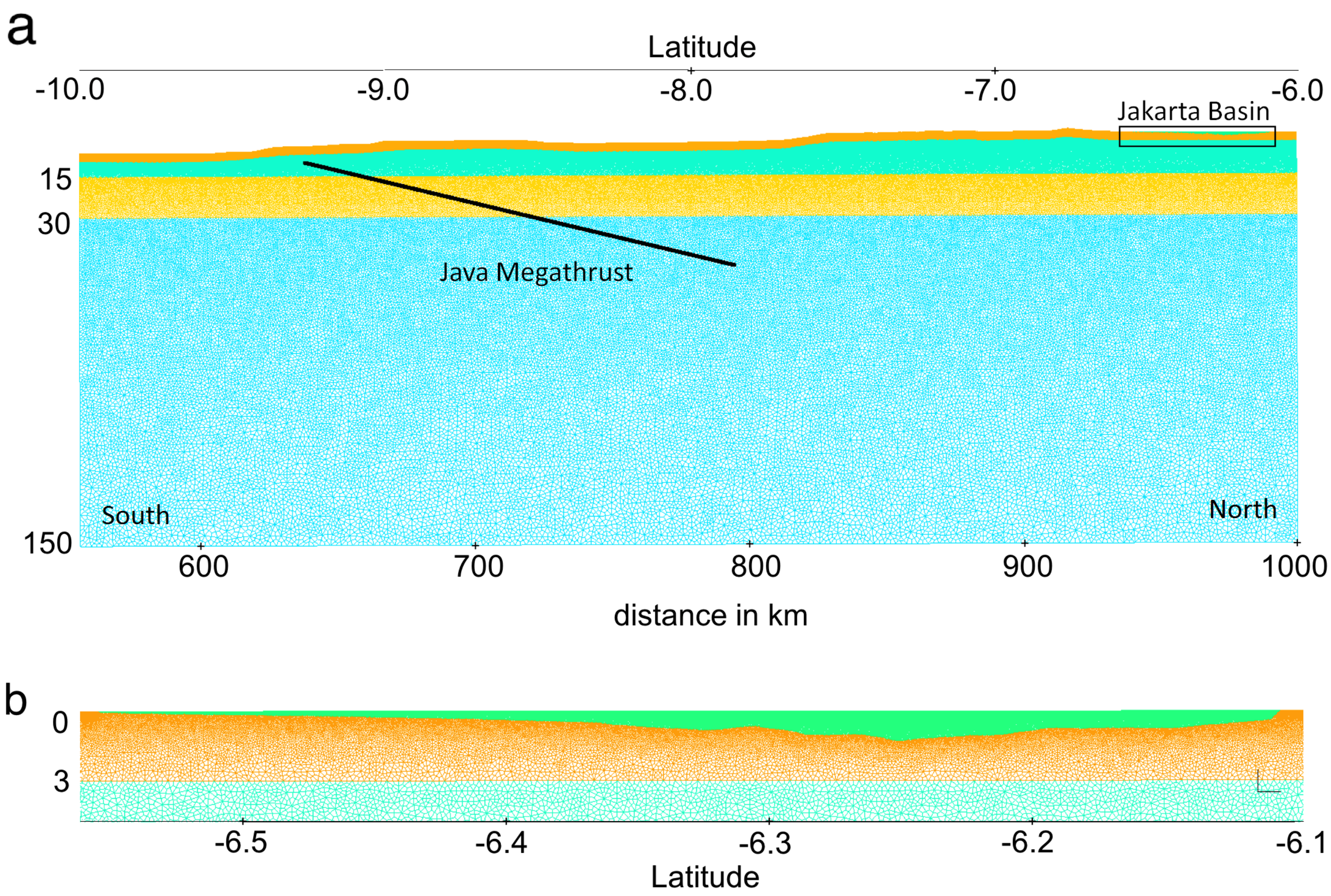

Figure 6. (**a**) The SPECFEM2D computational domain consists of a 5-layered medium, with the surface topography extracted from SRTM and the basin geometry resulting from the HVSR inversion. The vertical axis is depth (km) and horizontal is latitude in km and degree. The thick black line represents an inclined set of 1002 point sources along the subduction zone megathrust, and the area of the rectangle basin inset shown in (**b**) is indicated. For the crustal fault and deep intraslab scenarios, different dimensions of domain areas are used but the mesh-sizes for the first 4 top layers are same.

Peer-reviewed version available at *Geosciences* **2018**, *8*, 128; doi:10.3390/geosciences8040128

The total length of the computational domain for the megathrust event extends from 6° to 10° south latitude, the maximum depth is 150 km and highest elevation is 1.5 km. The topographic surface is extracted from the Shuttle Radar Topography Mission DEM (SRTM Digital Elevation Model, freely downloaded from: $https : //dds.cr.usgs.gov/srtm/ version2\_1/SRTM3/Eurasia/$). The domain area accommodates source locations and is divided into 5 zones including the basin, a 3-layer crust and the mantle. Irregular quadrangle meshes are generated to fill the domain area, the coarsest (maximum gridsize: 2000 m) meshes filling the lower layer while the finest meshes are arranged in the basin (maximum gridsize: 12.5 m). The very small mesh size in the basin, together with the large computational domain that includes the megathrust, results in a very large mesh size, of 800,000 elements. This large mesh size is the main reason that calculations in this study were limited to 2-D, as a 3-D mesh at this resolution would have resulted in very long computation time. The topographic surface is set to be a free surface while the other sides are set to be absorbent surfaces to avoid waves reflecting back into the domain area (see Figure 6).

While seismic attenuation in sedimentary basins like Jakarta can be high, we found that the viscoelastic calculations of SPECFEM2D for our large computational mesh were prohibitive (even the elastic calculations using 28 CPUs required a wall time of 18 hours; viscoelastic calculations took much longer). To our knowledge no studies of seismic attenuation or seismic quality factor for the Jakarta region have been undertaken, but in order to test the influence of attenuation we use Qp=44 and Qs=25, taken from a study conducted *Hauksson et al.* [23] in the Los Angeles Basin. Tests using these values for Qp and Qs in the basin indicated that viscoelasticity had a small effect for periods > 1 s. Therefore, in the simulations described here we neglected attenuation in the basin for reasons of computational efficiency. All parameters for simulations are presented in Table 1.

Table 1. Domain parameters used in simulation

layer	rho (kg.m^{-3})	V_P (ms^{-1})	V_S (m^{-1})	Q_κ^*	Q_μ^*	max depth (m)
Basin	1200	1600	582	44	25	1385
Layer 2	2200	4100	2300	283	150	3000
Layer 3	2900	5100	2800	450	450	13467
Layer 4	3200	6500	3200	500	500	15000
Layer 5	3800	8000	4000	600	700	120000

* Parameter values were tested but not used in the simulations presented here

In this study, we assume that seismic waves are generated outside the basin, in the Java subduction zone for the megathrust scenario, in the shallow crust to the south of the basin for the crustal earthquake scenario, and in the mantle for the intralsab scenario. Seismic waves propagate from the source through a 5-layer mantle + crustal model to the surface, as indicated in Table 1 On the surface, both inside and outside the basin, seismic waves will be recorded at stations located at 2 km spacing along a south-north cross-section. In order to account for 3-D geometrical spreading and attenuation in the crust and upper mantle in our 2-D elastic simulation, we scaled the computational results by matching the long-period (1-10 s) spectra of seismograms recorded just outside the basin with results from suitable GMPEs for the appropriate magnitude and distance. For the megathrust scenario, we scaled the seismograms by matching spectra with results of the AEA2014 GMPE, for the crustal source we used CY2014, and for the intraslab earthquake scenario we matched spectra to AEA2014S.

5. Results

5.1. GMPE modeling results

GMPE simulations have been performed and the results show that for PGA, pseudo spectral acceleration (PSA) at 0.2 s and 5.0 s, their patterns are very similar to each other, and closely follow the pattern of V_S30 input. At 5.0 s, which is close to the apparent resonance peak in most of the HVSR

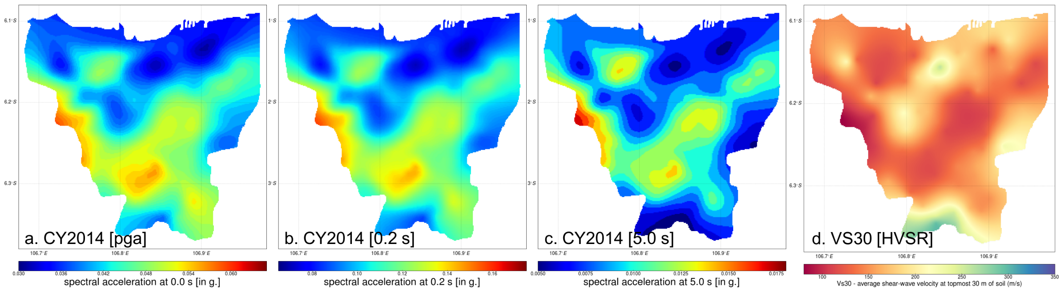

Figure 7. Comparison results of GMPE modeling using CY2014 for PGA, SA 0.2 s and SA 0.5 s (**a, b, c**). Eventhough $Z_{1.0}$ and $Z_{2.5}$ are included in the calculation, long period spectra (5.0 s) showing similar pattern to the V_S30 derived from HVSR (**d**). This indicates that basin depth term used in the GMPE may not adequately express the effects of basin geometry, at least for basins as deep as Jakarta's.

measured by *Cipta, et al.* [12], it is expected that basin geometry would have a significant influence on the long period ground motion. However, the effect of basin geometry is not really captured by yjr GMPE modeling as shown in Figure 7. For this reason, it seems clear that a more sophisticated approach is needed to account for basin effects in long period ground motions, at least until a GMPE specific for the Jakarta region is available.

5.2. Numerical Simulation Results

The crustal and megathrust events are situated south of Jakarta at distances 85 km and 200 km and with magnitudes M_w 6.5 and M_w 9.0, respectively. The megathrust is dipping north while the crustal fault is dipping south. The third scenario simulates propagation of seismic waves originating from a medium-depth intraslab earthquake located at the depth of the subducting slab at 180-204 km (fault width = 34 km) directly beneath the city. This fault is dipping south and the earthquake has magnitude M_w 7.0.

Snapshots from the crustal fault scenario are presented in Figure 8. After 10 s, the P-wave is showing up in the lower left corner of the topmost panel and at 12 s, both P-wave (dark) and S-wave (vermilion) are observed approaching the basin. At 50 s, seismic waves, both body and surface waves, have entered and are trapped inside the basin. Surface waves are modulated inside the basin and at 90 s, while body waves are attenuated and have faded away outside the basin, surface waves are still reverberating in the basin.

Seismograms (radial, horizontal component) resulting from these three scenarios are presented in Figure 9 **a-c**. Two types of seismograms are plotted: (1) those calculated using the elastic parameters indicated in Table 1, colored blue in Figure 9 and referred to here as 'basin seismograms', and those calculated using an identical computational mesh but with the basin elastic parameters replaced by those of the basement (i.e., the Basin parameters in Table 1 are replaced by those of Layer 2), colored orange in Figure 9 and referred to here as 'bedrock seismograms'. The three record sections in Figure 9 **a-c** clearly show that seismic waves propagating through the soft sediment inside the basin are amplified to different degrees. Outside the basin the orange colored curves (bedrock seismograms) match the blue curves (basin seismograms) perfectly, meaning that outside the basin, no amplification is observed. On the other hand, inside the basin, basin seismograms have much higher amplitudes and prolonged durations in comparison to bedrock seismograms. It is interesting to note that the basin-bedrock seismogram ratio is not uniform, and basin depth is not the only factor contributing to the amplification. Basin geometry and direction of incoming waves also appear to influence the degree of amplification.

For the crustal earthquake scenario, Figure 9 **a**, seismic waves propagating toward the north edge of the basin are reflected back into the basin and recorded at 200 s at the southernmost station (S2117) and at progressively earlier times at more northerly stations. However, at S2157 to S2176, reflected

Peer-reviewed version available at Geosciences 2018, 8, 128; doi:10.3390/geosciences8040128

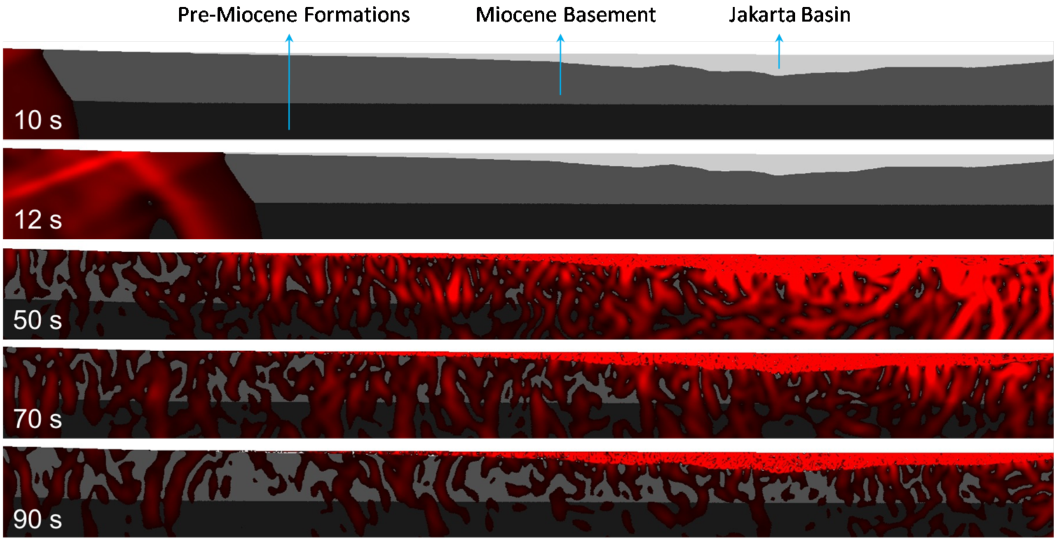

Figure 8. Snapshots of wave propagation, showing waves approaching (10 and 12 s, top two panels) and reverberating inside (50, 70 qnd 90 s, bottom three panels) the basin. The modeled M_w 6.5 earthquake is taken to have ruptured a southward dipping, shallow crustal thrust fault 85 km south of the city center. The Jakarta Basin is the light gray colored area, overlying the dark grey medium, clearly shown in the top two pictures capturing snapshots at 10 and 12 s, respectively.

waves are not clearly seen because they interfere with seismic waves propagate northward, producing high amplitude seismograms at 50-60 s (Figure 5.14a). The megathrust earthquake also exhibits reflected waves that are clearly observed at S2130 to S2169, again with reflected waves recorded earlier in the north than in the south (Figure 9**b**).

In contrast to the other two scenarios, the intraslab earthquake scenario shows reflected waves from both south and north edges. Near the south edge, high amplitude seismic waves are observed at stations S2130-2135 at times 50-100 s. These high amplitudes are generated from interaction between incoming and reflected waves as well as entrapment at the basin's edge. As time goes by, waves reflected by the northern edge of the basin are recorded after 100 s in the southern stations and recorded earlier in the central and northern stations.

Seismograms in Figure 10**a-b** record incoming P- and S-waves at 20 s and 36 s, respectively, for the crustal fault scenario. For the basin seismograms in Figure 10**c-d**, the direct S-wave is followed by a series of reverberations comprised of S-wave and Rayleigh wave energy, that builds up over the following 15 s, with the highest vertical component amplitude achieved 10 s after the direct S-wave arrival. It is observed that S-wave/Rayleigh wave coda that builds up at about 37 s is still observed after more than 150 s. The bedrock seismograms (Fig 10**e-f**) are dominated by the direct S-wave and have a very weak coda after only a few seconds.The long duration ($>$ 120 s) and very high amplitude of basin seismic waves after 40 s indicatse the interference between seismic body waves and surface waves.

The intraslab scenario produces similar results, at the same station, with surface waves observed after 55 s and still trapped inside the basin after 240 s. In the case of the megathrust event, the Rayleigh wave arrives about 25 s after the P-waves recorded in the seismograms. The interference of reverberating surface waves leads to very high amplitudes, compared to the crustal and intraslab scenario. Entrapment of seismic waves inside the basin prolongs the duration of seismic waves, with high amplitude seismic waves still observed 10 minutes after the earthquake. Interference between seismic body waves and secondary surface waves was recognized as a main cause of building collapse in Kobe during the 1995 Great Hanshin Earthquake (*Zhao et al.* [51]).

Peer-reviewed version available at *Geosciences* **2018**, *8*, 128; doi:10.3390/geosciences8040128

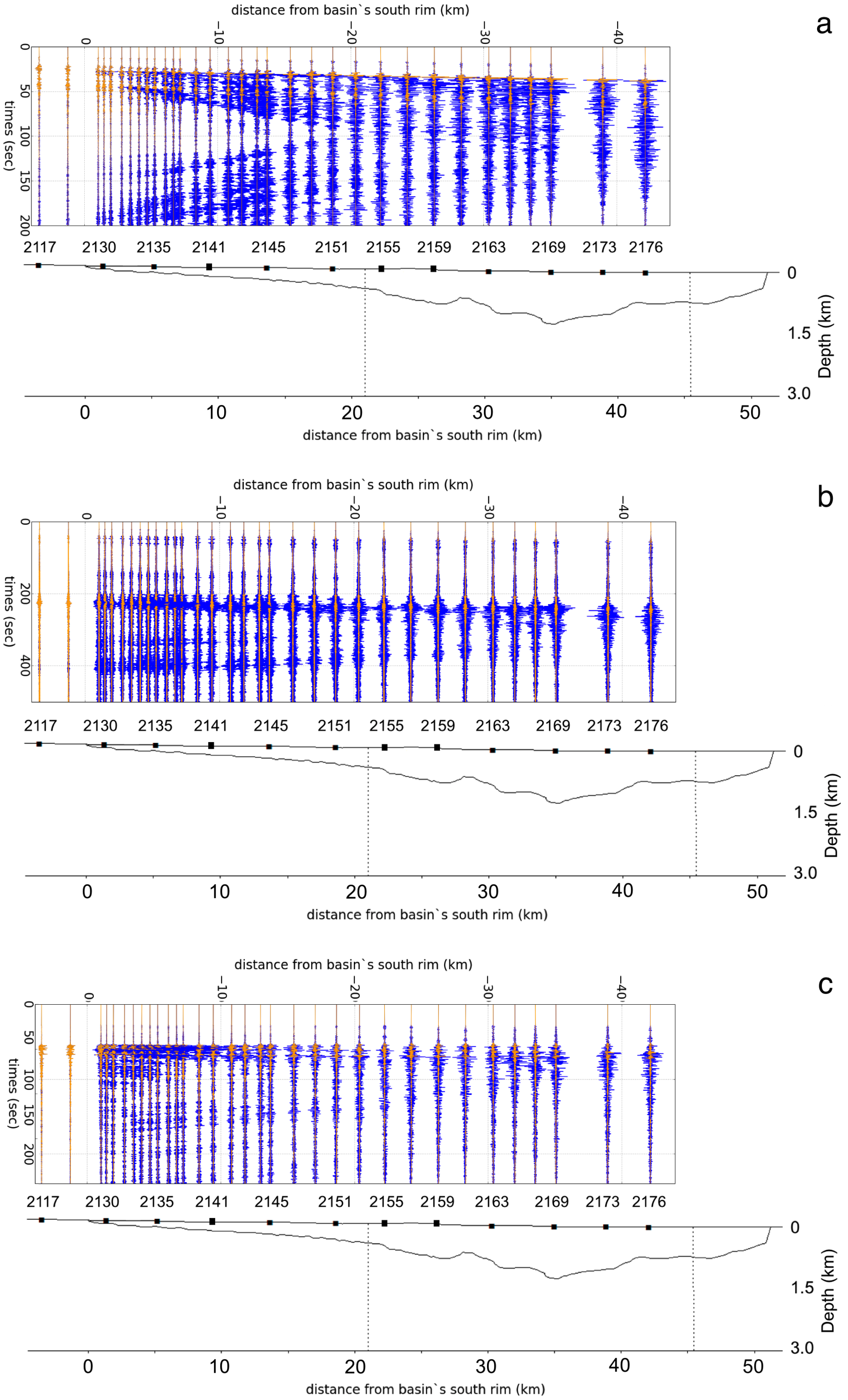

Figure 9. Bedrock seismograms (orange traces) are plotted over basin seismograms (blue traces.) Outside the basin, no amplification has occurred, while inside the basin high amplifications and prolonged durations are observed. The level of amplification is different from station to station and depends upon geometry of the basin. Labelled points indicate location of stations correspond to the seismograms plotted directly above the points. In the area between dotted lines (21-41 km from the basin's rim) basin structure inferred from *Cipta, et al.* [12] while the extension of the basin is estimated from geological data.

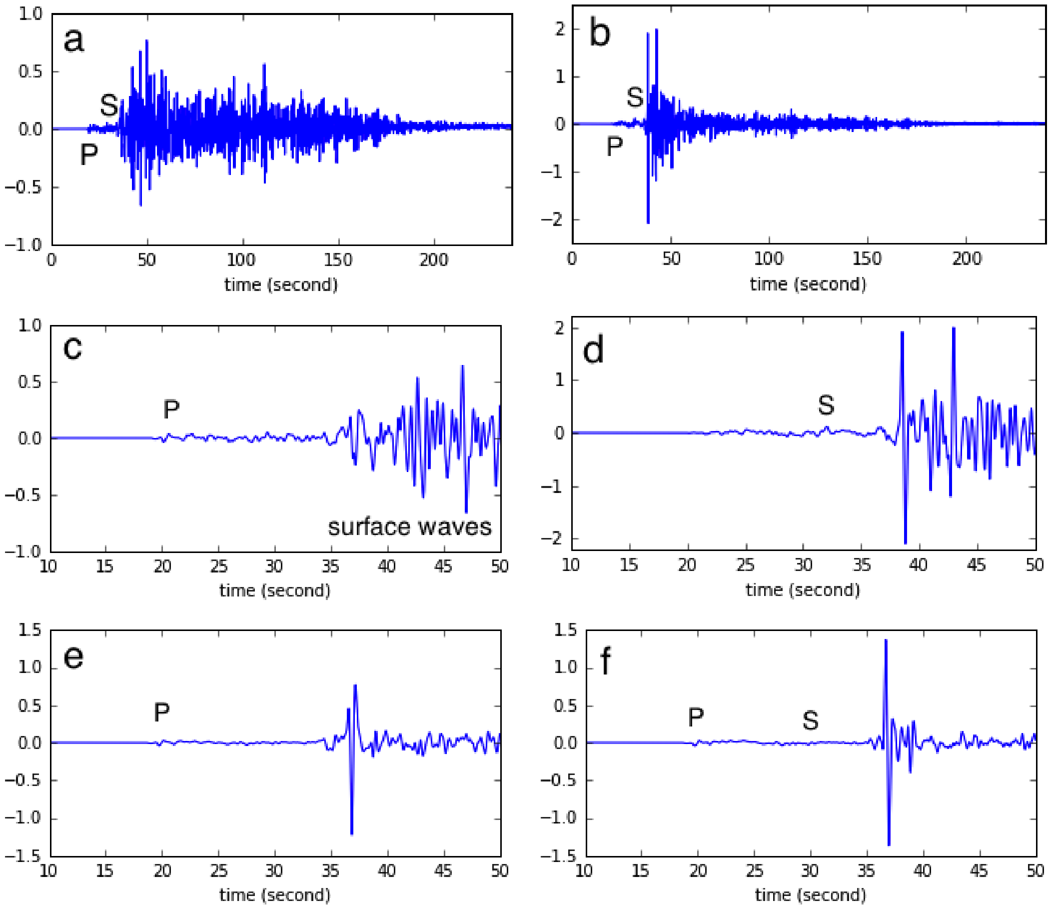

Figure 10. Seismograms at stations S2169, both for vertical (**a**) and horizontal (**b**) components, showing P-, S- and surface waves generated from the crustal fault scenario. Figs. **c** and **d**: the same seismograms at time 10-50 second, showing the arrival of direct S followed by Rayleigh surface waves at about 37 s. Similar to **c** and **d**, **e** and **f** are seismograms recorded at bedrock sites. For a clearer image, Y-axes are magnified differently for each figure, so values at Y-axes do not show actual units.

The three scenarios indicate that the larger the magnitude, the longer the seismic waves were observed inside the basin. The "red" (i.e., long-period dominant) spectrum of frequency content generated by the larger rupture area may be responsible for the very long duration of long period ground motions generated by the megathrust scenario. Together with the maximum amplitude and duration of seismic waves, frequency content is also a very important factor that is responsible for building damage. According to *Shoji et al.* [44], duration is more event-dependent than site-dependent while the site-dependency for a given total power is greater than the event-dependency.

6. Discussion

6.1. GMPE - Seismic Hazard

Using GMPE modeling, psuedo-spectral acceleration (PSA) for each spectral period can be computed and by taking the maximum PSAs over the basin, simulated response spectra (SRS) can be generated. SRS from each scenario can be compared to the designed response spectrum used for the building code in Jakarta to investigate the performance of the building code. However, since GMPE simulations do not fully take the effects of basin geometry into account, longer period PSA may be underestimated, and hence we need to be careful in interpreting the curves presented in Figure 11.

Peer-reviewed version available at Geosciences 2018, 8, 128; doi:10.3390/geosciences8040128

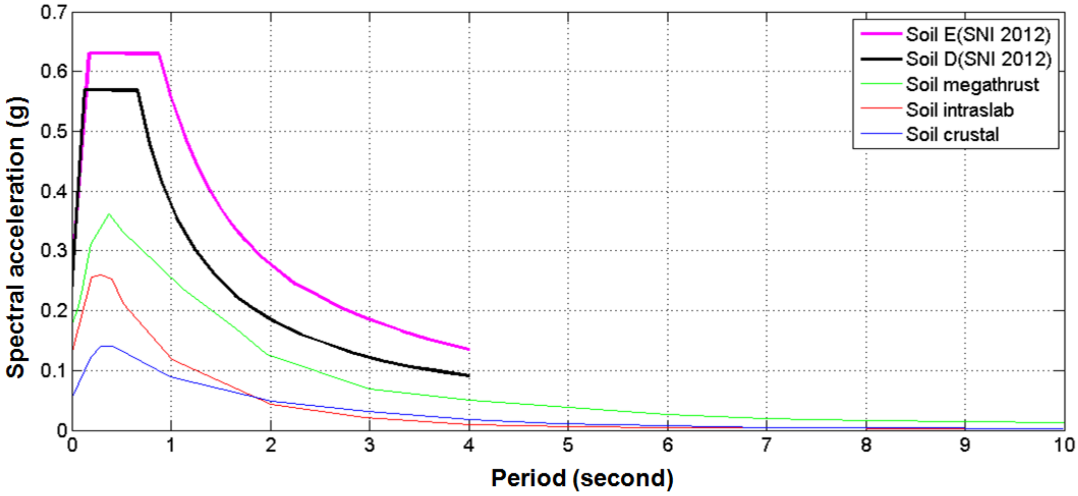

Figure 11. Design response spectrum used for the 2012 Indonesian Building Code for medium soil sites in Jakarta (thick black curve). Also plotted are acceleration response spectra produced from GMPE simulations for crustal fault (GMPE:CY2014), megathrust (GMPE:AEA2015) and intraslab earthquake (GMPE:AEA2015S) scenarios (blue, green and red curves, respectively), calculated on soil sites.

For this reason, let us compare design seismic response and SRS at the shorter periods (< 1 s) only, and note that shorter period response spectra correspond to the natural resonance of most residential buildings (which, however, are not generally required to conform to the Indonesian building code)

A very important characteristic of seismic waves is their period. This phenomenon is particularly important for determining building response to seismic forces. Buildings have a natural or fundamental period, corresponding to the resonant period at which a building sways back and forth in a horizontal direction. In fact, without being subject to significant external force, a building vibrates only at its natural period. When the building is subject to an external force, by for example horizontal ground motion or wind, whose period matches the building's natural period, the building may experience resonance that enhances building vibration by as much as 4–5 times (*Arnold et al.* [6]).

To estimate the natural period of a building with respect to its height or number of stories, for a reinforced concrete building, the following equation can be used (e.g. *UBC* [48] and *Wiegel* [50]):

$$T_n = C_t \times h^{3/4} \tag{2}$$

where T_n and h denote spectral period (in second) and height of a building in meters, respectively, while C is a coeficient that accounts for the number of storeys, height of building and amount of infilled panel. This coefficient varies from 0.05 (*Wiegel* [50]) to 0.073 (*UBC* [48]) if the height is in meters. For practical purposes, the above equation can be simplified as follows: the natural period of a building is equal to the number of storeys divided by 10 *Arnold et al.* [6]. For example, a common residential building composed of 1–3 stories will be most sensitive to ground motion at spectral periods in the range 0.1-0.3 s.

The current building code (2012 Indonesia's National Standard–SNI 1726-2002) adopted the updated seismic map of *Irsyam et al.* [24] that estimated ground motions for a 2% probability of exceedance in 50 years (2500 years return period) as the maximum considered earthquake (MCE) level. Figure 11 shows that the current seismic building code in Indonesia that takes into account D and E soil classes performs well against the PSA estimated from GMPEs for all 3 scenarios. In this figure, the thick black and magenta curves represent designed ground motion produced by the MCE in a 2500 years return period for D- and E-type soils, respectively.

6.2. Numerical Simulations - Peak Ground Velocity (PGV)

Numerical simulation of seismic waves using SPECFEM2D for selected earthquake scenarios is an approach that should give a more complete account of basin and site effects than is obtainable form GMPEs. Three scenarios, namely, crustal, megathrust and intraslab scenarios are considered. These simulations are conducted to estimate the long period ground motions which are affected by basin resonance that may not be accounted for by the GMPE modeling considered above.

The Mw 6.5 crustal fault scenario generates a maximum peak ground velocity of 0.038 m/s and maximum PGV amplification is about 206%. Figure 12**a** shows that amplification is not uniform throughout the basin; at station S2147, amplification is small (about 20%), while other stations recorded higher velocities due to amplification. Most striking is the amplification observed at S2169 at the deepest part of the basin (Figure 12 and Figure 13**a-c**). Amplification here is describe in a manner similar to that used by *Pilz et al.* [38] in calculating estimated PGV amplification in Santiago Basin, Chile: we subtract the PGV values for the bedrock seismograms from the value for the basin seismograms, and divide this by the PGV value for the bedrock seismograms (multiplying by 100 to convert to percentage amplification).

Different characteristics of simulated PGV and amplification are produced by the megathrust earthquake scenario. PGV and amplification tend to increase as the basin gets deeper. Prominent PGV and amplification are recorded at stations S2153 and S2173. Simulated PGV at these stations are 0.683 m/s and 0.714 m/s while amplifications are 579% and 687%, respectively (Figure 12**a** and Figure 13**d-f**).

The intraslab earthquake scenario results in very high amplification, especially at S2131, so that the estimated PGV in that station is higher than the other stations. The source of the intraslab scenario is very deep and directly beneath the city, so that rupture-to-station distance is the same for all stations, hence the variation of amplification with respect to rupture distance can be neglected. Therefore, high amplification at this station is most probably due to focusing of seismic waves by the basin edge, while entrapment of seismic waves inside the basin may also affect amplification at this station. High amplification is also recorded at S2165, where particulary thick basin fill is responsible for high amplification (Figure 12**a** and Figure 14**a-c**). Recorded PGV (m/s) and amplification (%) for all three scenarios are presented in Table 2. Minor amplification or deamplification recorded at stations S2117 and S2124 that are located outside the basin may come from simulation noise.

6.3. Numerical Simulation - Response Spectral Acceleration

The megathrust scenario generated the highest peak ground velocity and amplification in the basin, especially at station S2173. In this section, we will look at the response spectral acceleration that is widely used to characterise ground motion in civil engineering, then compare the design building code against spectral acceleration resulting from SPEFEM2D modeling. At station S2169 and S2173, simulated horizontal acceleration at period 1 s are about 0.45 g, which is higher than the design response spectrum used by the building code. At periods shorter than 1 s very high accelerations are observed (Figure 15), however, these results may be inaccurate since neither near surface attenuation κ nor crustal and basin frequency-dependent attenuations for V_P and V_S (Qp and Qs) for Jakarta region are available.

Since long period (>1 s) ground motions are much less sensitive to κ, Qp and Qs, it seems reasonable to consider how these compare to the design response spectrum. At S2161, there are two ground motion peaks that fall on or above the design response spectrum, at periods of about 1.5 s and 3.5 s (Figure 15**a**)..

For the intraslab earthquake scenario, basin edges effects can be particularly pronounced as observed in Figure 9 **c**. Amplification of short period ground motions, particularly at periods of about 0.55 s, result in very high acceleration (3 g) at S2131 (16). At this point, the PGV amplification is 335% (14), but this high frequency content may not be realistic due to the lack of consideration of attenuation effects as discussed above. On the other hand, the high amplification at S2165 in the deepest part of

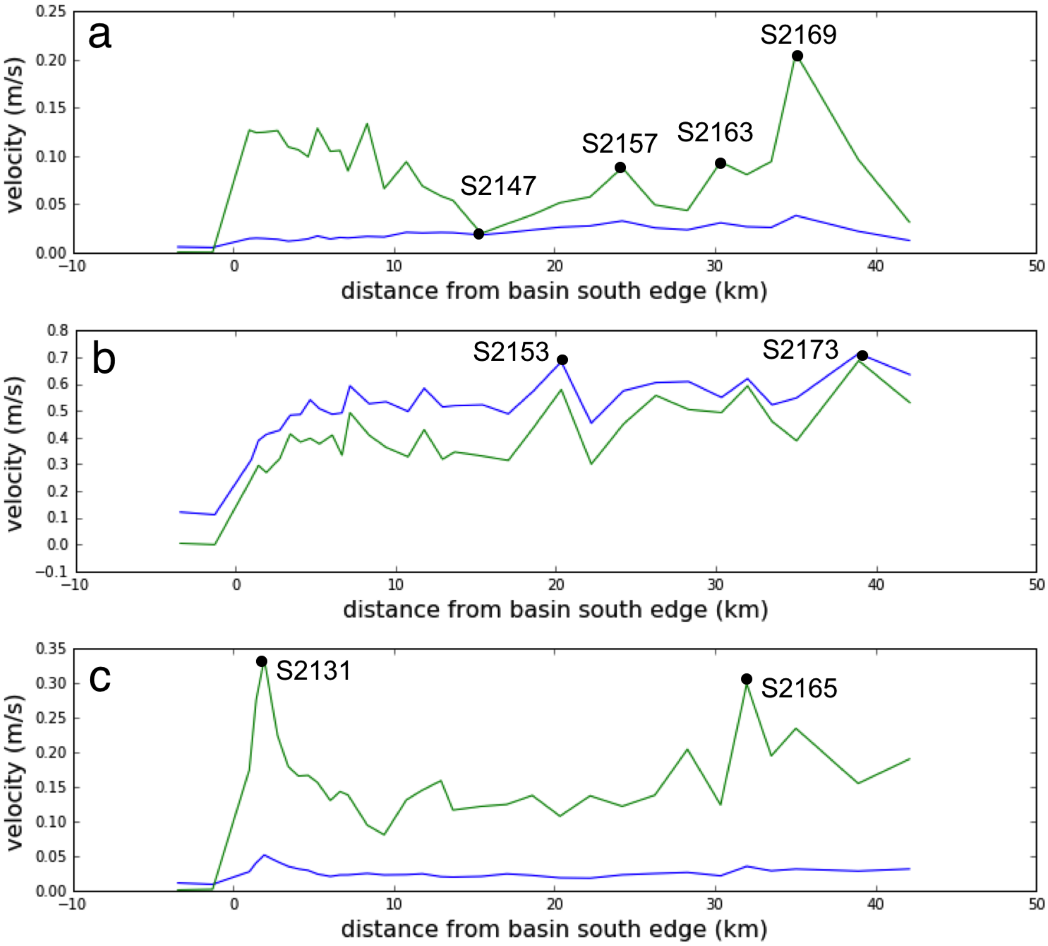

Figure 12. Peak velocity at stations plotted as a function of distance from the basin edge, generated for crustal fault (1), megathrust (b), and intraslab (c) earthquake scenarios. Blue and green curves represent peak velocity in the basin stations and amplification (percentage amplification divided by1000), respectively. Selected stations name are indicated by labelled dots.

Table 2. Amplification in % resulted from 3 scenarios

Station	PGV-C	Ampli-C	PGV-M	Ampli-M	PGV-S	Ampli-S
S2117	0.006	0	0.121	4	0.011	1
S2124	0.005	0	0.111	-1	0.009	2
S2129	0.014	127	0.317	246	0.027	174
S2130	0.015	124	0.388	295	0.040	277
S2131	0.014	125	0.412	269	0.051	335
S2132	0.013	126	0.427	320	0.042	224
S2133	0.012	109	0.483	414	0.035	180
S2134	0.013	106	0.486	383	0.031	166
S2135	0.014	99	0.541	397	0.029	167
S2136	0.017	129	0.508	376	0.024	156
S2137	0.014	105	0.487	409	0.020	131
S2138	0.015	106	0.492	334	0.022	143
S2139	0.015	85	0.593	493	0.023	138
S2140	0.017	134	0.526	409	0.025	95
S2141	0.016	66	0.534	363	0.023	81
S2142	0.021	94	0.497	328	0.023	131
S2143	0.020	69	0.584	429	0.024	145
S2144	0.021	58	0.514	318	0.020	159
S2145	0.020	54	0.519	346	0.019	116
S2147	0.018	20	0.522	330	0.020	122
S2149	0.020	30	0.488	314	0.024	125
S2151	0.023	39	0.575	438	0.022	138
S2153	0.026	51	0.683	579	0.018	108
S2155	0.027	58	0.454	300	0.018	137
S2157	0.033	88	0.575	450	0.023	122
S2159	0.025	49	0.605	557	0.025	138
S2161	0.023	44	0.609	505	0.026	205
S2163	0.031	94	0.550	493	0.021	124
S2165	0.027	81	0.620	593	0.035	299
S2167	0.026	94	0.522	460	0.029	195
S2169	0.038	206	0.548	388	0.031	235
S2173	0.022	96	0.714	687	0.028	155
S2176	0.012	32	0.635	530	0.031	190

PGV-C, PGV-M, PGV-S, Ampli-C, Ampli-M, Ampli-S are peak ground velocity (PGV) and amplification (Amp) generated from crustal fault, megathrust and intraslab scenarios. PGV and amplification are in units of m/s and %.

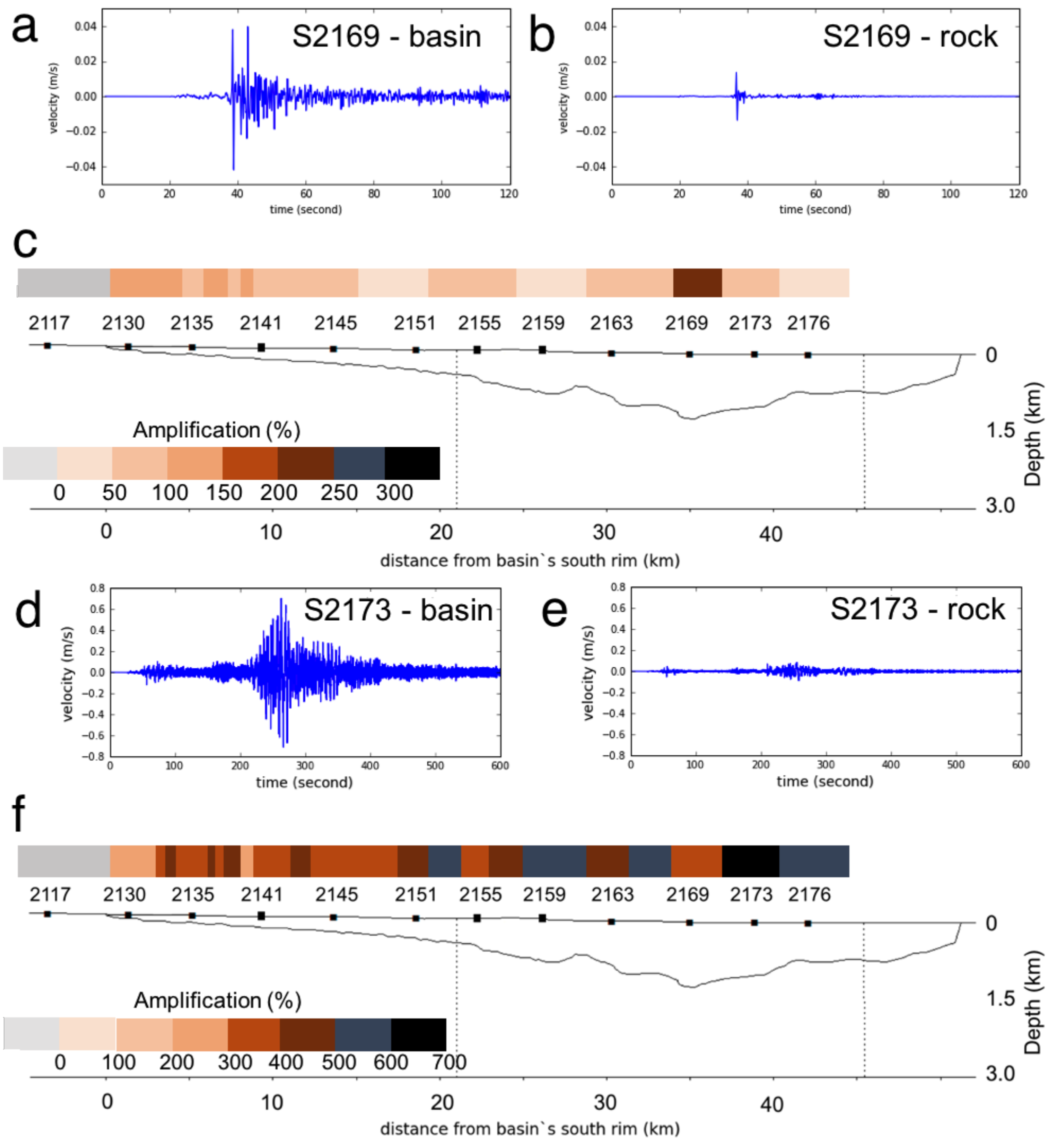

Figure 13. amplification for the crustal (a-c) and megathrust (d-f) earthquake scenarios. Figures **a, b** show velocity seismogram at stations S2169 for basin and bedrock sites respectively, and Figure **c** shows PGV amplification at each station along the S-N cross-section for the crustal fault scenario. Similar to Fig **a, b, c**, Fig **d, e, f** depict seismograms at basin and rock sites (S2173) and PGV amplification for the megathrust earthquake scenario. The cross-section is located at the longitude 108.84335° and seismograms are the raidial horizontal component.

Peer-reviewed version available at *Geosciences* **2018**, *8*, 128; doi:10.3390/geosciences8040128

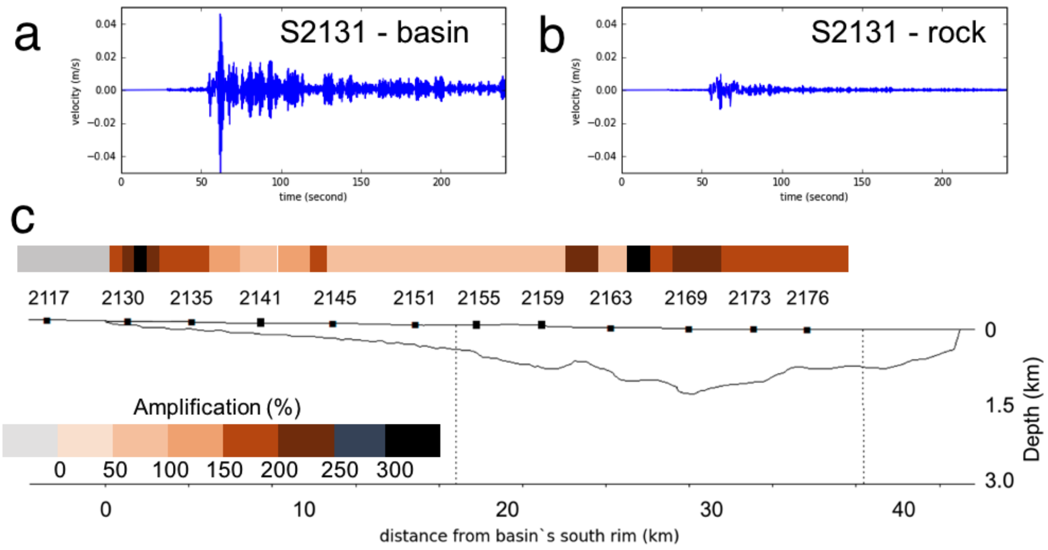

Figure 14. Similar to Figure 13 , but for medium-depth intraslab earthquake scenario. Figure **a, b** are basin and bedrock seismograms (at S2131, located about 500 m north of S2130) and Figure **c** shows PGV amplification along the S-N cross-section.

the basin as can be seen in Figure 12c, is apparent in ground motion at about 1 s period, as shown in Figure 16, which is not strongly affected by attenuation. The spectral amplification at this point is as high as 424% or slightly higher than the PGV amplification (300%). More interesting features appear at the longer periods. While long period (> 1 s) accelerations at S2131 fall below the 2012-SNI design response spectrum, at S2165 the scenario response spectrum at about 5.5 s is touching the design response spectrum. An acceleration of 0.06 g and amplification of 335% (for period of 5.5 s) are estimated by the simulation (Figure 16).

7. Conclusion

We have shown that GMPE modeling predicts the significant influence of near-surface geology, represented by V_S30, , on short-period (< 1 s) seismic waves. However, for a very deep basin filled with soft sediment, available GMPEs are not capable of capturing the effects of basin geometry on seismic waves, at least for basins as deep as the Jakarta Basin. Consequently, more realistic approaches should be used to estimate ground motions. SPECFEM2D was chosen to simulate earthquake scenario ground motions, and the results show how soft sediment filling a deep basin amplifies seismic waves, generating high ground motion on the basin surface.

The amplification of ground motion due to basin geometry and depth varies from site to site, and depends upon depth of the basin, distance from the source, distance from the basin edge and also magnitude of the earthquake. While the megathrust scenario showed a close correspondence between PGV and spectral amplification, the crustal fault and especially intraslab scenarios showed a more complex relationship. These latter scenarios show high amplification in the south and north parts of basin and show low amplification in the central part. Highest PGV are observed at the north stations, where the basin is very deep (>1000 m), in the crustal fault and megathrust scenarios. In contrast, the intraslab scenario triggered the highest PGV near the basin edge.

The crustal fault scenario produced high spectral amplitudes at frequencies in the range 0.4-0.6 Hz, while the megathrust event generated high ground motions at frequencies of about 0.2 Hz and 0.5 Hz (15). Pronounced high ground motions at frequencies about 0.2 Hz are generated by the deep intraslab scenario (16). The high spectral amplitudes in the period range of 1.6-10 s are approximately in accordance with natural periods of 16–100 story buildings, therefore, basin resonance may be a more important consideration for high-rise buildings construction than previously realised.

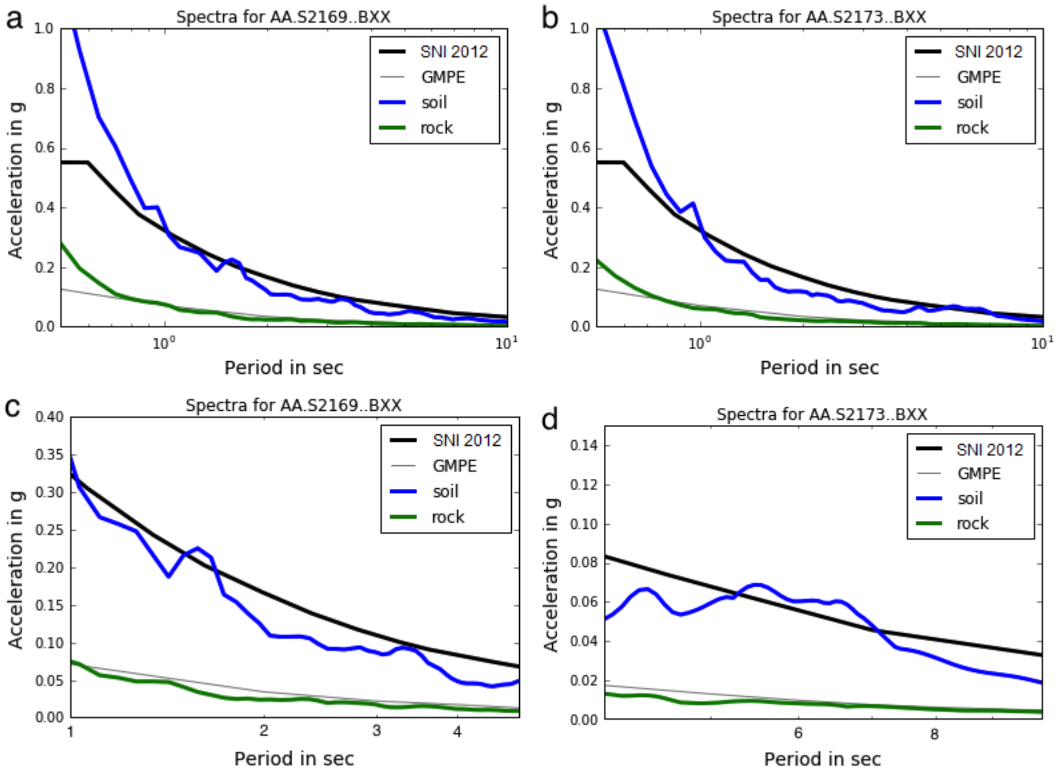

Figure 15. Computed acceleration response spectra for the megathrust earthquake scenario, plotted with the PSA using the AEA2015 GMPE and the Jakarta Building Code's design response spectrum (for D-type soil, thick-black curve) at stations S2169 (**a**) and S2173 (**b**). (**c**) and (**d**) are zoomed images of (**a**) and (**b**), respectively for the period band 1-5 s (**c**) and 4-10 s (**d**). Location of stations are indicated in Figure 13 and Figure 14

Megathrust earthquakes may trigger high spectral accelerations in Jakarta. Especially at a period of 1 s, the simulated acceleration is higher than the design spectrum of the building code. At some stations (e.g. S2173), acceleration at about period 5 s is also a bit higher than the building code's design spectrum. This high acceleration and long duration of seismic waves inside the basin, as shown in Figure 5.14, should be of concern, because these factors can be responsible for building collapse. The high spectral accelerations (0.07-0.08 g) at periods between 5-7 s are estimated from the megathrust scenario, but high spectral acceleration (0.06 g) at a period of about 5.5 s is also estimated due to the intraslab earthquake scenario.

While results in this study should be regarded as preliminary in that they neglect the effects of attenuation inside the basin and do not account for 3-D wave propagation, overall they show the greatly enhanced seismic hazard in Jakarta due to its deep basin structure. When this is combined with Jakarta's proximity to earthquake sources (megathrust and active faults) and destructive earthquakes that have devastated Jakarta centuries ago, the risk of catastrophic damage should one of these large historical events occur today seems very real.

Acknowledgments: Computations were performed on the Raijin cluster of the Australian Computational Infrastructure Facility. This work was partially supported by the Australian Department of Foreign Affairs and Trades Grant 91982 and the Australian Research Council (ARC) Linkage Grant LP110100525. A.C. was supported by a scholarship from the Indonesian Ministry of Energy and Mineral Resources (MAK 020.01.01.1881.002.001.012 A.521219).

Author Contributions: A.C. performed the bulk of the analysis and numerical simulations; P.C. provided overall guidance and technical support for the numerical simulations and analysis; M.I. provided advice on earthquake engineering aspects and the Indonesian building code; S.H. provided advice on geology of the Jakarta Basin.

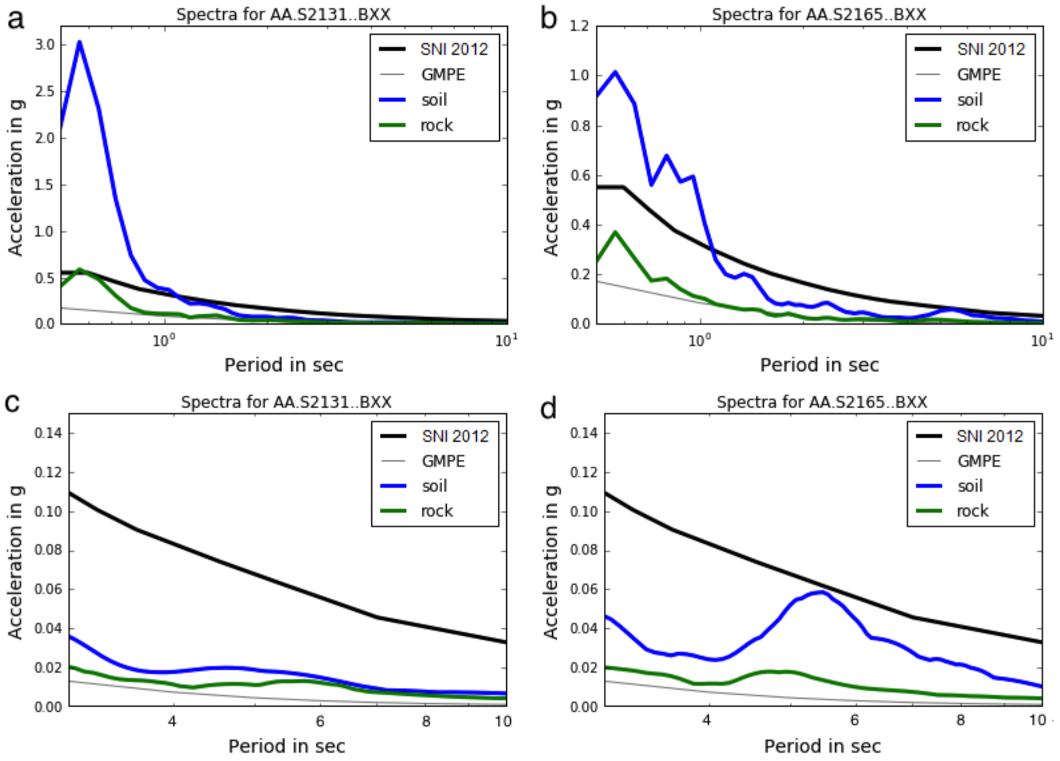

Figure 16. Computed acceleration response spectra for the intraslab earthquake scenario, plotted with the PSA using the AEA2015S GMPE and the Jakarta Building Code's design response spectrum (for D-type soil, thick-black curve) at stations S2131 (**a**) and S2165 (**b**). (**c**) and (**d**) are zoomed images of (**a**) and (**b**), respectively, for the period band 3-10 s. Locations of S2165 are indicated in Figure 5.19 and Figure 5.20, while S2131 is 500 m north of S2130 in the same figures. Note, that the Y-axes have different scales.

Conflicts of Interest: The authors declare they have no conflict of interest."

Peer-reviewed version available at Geosciences 2018, 8, 128; doi:10.3390/geosciences8040128

1. Abidin, H. Z., H. Andreas, T. Kato, T. Ito, I. Meilano, F. Kimata, D. Natawidjaja, and H. Harjono (2009). Crustal deformation studies in Java (Indonesia) using GPS. *J. Eq. Tsu.* **3(2)**, 77–88.
2. Abidin, H. Z., H. Andreas, I. Gumilar, Y. Fukuda, Y. E. Pohan and T. Deguchi (2011). Land subsidence of Jakarta (Indonesia) and its relation with urban development. *Nat. Hazards* **18**, 232–242.
3. Abrahamson, N. A., N. Gregor and K. Addo (2016). BC Hydro Ground Motion Prediction Equations for Subduction Earthquakes. *Earthquake Spectra* **32(1)**, 23–44.
4. Albini, P., R. M. W. Musson, A. A. Gomez Capera, M. Locati, A. Rovida, M. Stucchi, and D. Viganó. (2013). *Global Historical Earthquake Archive and Catalogue (1000-1903)*. Pavia, Italy.
5. Allmendinger, R. W. (2017). *Modern Structural Practice: A structural geology laboratory manual for the 21st Century v.1.7.0 ©2015-2017*. http://www.geo.cornell.edu/geology/faculty/RWA/structure-lab-manual/.
6. Arnold, C., B. Bolt, D. Dreger, E. Elsesser, R. Eisner, W. Holmes, G. McGavin, and C. Theodoropoulos (2006). *Risk Management Series: Designing for Earthquakes, A Manual for Architects* Earthquake Engineering Research Institute (EERI) of Oakland, California, FEMA/DHS.
7. Bard, P. Y. and M. Bouchon (1985). The two-dimensional resonance of sediment-filled valleys *Bull. Seism. Soc. Am.*, **75(2)**, 519–541.
19. GEM Foundation (2014). Openquake source code. https://www.globalquakemodel.org/
9. Brinkhoff, T. (2017). City Population. http://citypopulation.de/world/Agglomerations.html
10. Campbell, K.W., and Y. Bozorgnia (2013). NGA-West2 Campbell-Bozorgnia Ground Motion Model for the Horizontal Components of PGA, PGV, and 5%-Damped Elastic Pseudo-Acceleration Response Spectra for Periods Ranging from 0.01 to 10 sec. *PEER*, Report No. 2013/06.
11. Campbell K. W. and Y. Bozorgnia (2014). NGA-West2 Ground Motion Model for the Average Horizontal Components of PGA, PGV, and 5% Damped Linear Acceleration Response Spectra. *Earthquake Spectra* **30(3)**, 1087–1115.
12. Cipta, A., P. Cummins, J. Dettmer, E. Saygin, M. Irsyam, A. Rudyanto, and J. Murjaya (2018). Seismic Velocity Structure of the Jakarta Basin, Indonesia, using Trans-dimensional Bayesian Inversion of Horizontal-to-Vertical Spectral Ratios. *Submitted to Geophys. J. Int.*
13. Chiou, B., and R. Youngs (2014). Update of the Chiou and Youngs NGA Model for the Average Horizontal Component of Peak Ground Motion and Response Spectra. *Earthquake Spectra* **30(3)**, 1117–1153.
14. Cruz-Atienza, V. M., J. Tago, J. D. Sanabria-Gómez, E. Chaljub, V. Etienne, J. Virieux, and L. Quintanar (2016). Long Duration of Ground Motion in the Paradigmatic Valley of Mexico. *Nature* **6(38807)**.
15. Dardji, N., T. Villemin, and J. P. Ramnoux (1994). Paleostresses and strike-slip movement: the Cimandiri Fault Zone, West Java, Indonesia . *J. SE Asian E. Sc.* **9(1/2)**, 3 – 11.
16. Furumura, T. and L. Chen (2005). Parallel simulation of strong ground motions during recent and historical damaging earthquakes in Tokyo, Japan. *Parallel Computing* **31(2)**, 149–165.
17. Galetzka, J., D. Melgar, J. F. Genrich, J. Geng, S. Owen, E. O. Lindsey, X. Xu, Y. Bock, J.-P. Avouac, L. B. Adhikari, B. N. Upreti, B. Pratt-Sitaula, T. N. Bhattarai, B. P. Sitaula, A. Moore, K. W. Hudnut, W. Szeliga, J. Normandeau, M. Fend, M. Flouzat, L. Bollinger, P. Shrestha, B. Koirala, U. Gautam, M. Bhatterai, R. Gupta, T. Kandel, C. Timsina, S. N. Sapkota, S. Rajaure, N. Maharjan (2015). Slip pulse and resonance of the Kathmandu basin during the 2015 Gorkha earthquake, Nepal. *Science* **349(6252)**, 1091–1095.
18. García, D., S. K. Singh, M. Herraíz, M. Ordaz, and J. F. Pacheco (2005). Inslab Earthquakes of Central Mexico: Peak Ground-Motion Parameters and Response Spectra. *Bull. Seism. Soc. Am.* **95(6)**, 2272–2282.
19. GEM Foundation (2014). Openquake source code. https://www.globalquakemodel.org/
20. Graves, R. W., A. Pitarka, and P. Sommerville (1998). Ground-motion amplification in the Santa Monica area: Effects of shallow basin-edge structure. *Bull. Seism. Soc. Am.* **88(5)**, 1224–1242.
21. Hall, R. (2009). Hydrocarbon basins in SE Asia: understanding why they are there. *Petroleum Geoscience* **15**, 131–146.
22. Handayani, L., Maryati, Kamtono, M. M. Mukti, and Y. Sudrajat (2017). Audio-Magnetotelluric Modeling of Cimandiri Fault Zone at Cibeber, Cianjur. *Indonesian Journal on Geoscience* **4(1)**, 39–47.
23. Hauksson, A., T. L. Teng, and T. L Henyey (1987). Results from a 1500 m Deep, Three-level Downhole Seismometer Array: Site Response, Low Q values and f_{max}. *Bull. Seism. Soc. Am.* **7(6)**, 1883–1904

24. Irsyam, M., Sengara, W., Aldiamar, F., Widiyantoro, S., Triyoso, W., Hilman, D., Kertapati, E., Meilano, I., Suhardjono, S., Asrurifak, M. and M. Ridwan (2011). Development of Seismic Hazard Maps of Indonesia for Revision of Seismic Hazard Map in SNI 03-1726-2002. Research Report: *Indonesian Ministry of Public Works*
25. Kingston, J. (1988). Undiscovered petroleum resources of Indonesia. Open-File Report: *USGS* 88-379
27. Komatitsch, D. and J. P. Vilotte (1998). The spectral element method: an efficient tool to simulate the seismic response of 2D and 3D geological structure. *Bull. Seism. Soc. Am.* **88(2)**, 368–392.
27. Komatitsch, D. and J. P. Vilotte (1998). The spectral element method: an efficient tool to simulate the seismic response of 2D and 3D geological structure. *Bull. Seism. Soc. Am.* **88(2)**, 368–392.
28. Koulali, A., S. McClusky, S. Susilo, Y. Leonard, P. Cummins, P. Tregoning, I. Meilano, J. Efendi, A. B. Wijanartob (2017). The kinematics of crustal deformation in Java from GPS observations: Implications for fault slip partitioning. *Earth and Planetary Science Letters* **458**, 69–79.
29. Marafi, M. A., M. O. Eberhard, and J. W. Berman (2017). Effects of the Yufutsu Basin on Structural Response during Subduction Earthquakes. *Proceeding: the 16thWCEE 2017)* No. 2629.
30. Marliyani G. I. and Arrowsmith, R. (2014). Tectonic Geomorphology of the Hanging Wall Blocks of the Cimandiri Fault Zone, West Java, Indonesia. *Abstract: AGU, Fall Meeting 2014*, **T41C-4650**.
31. Meilano, I., H. Z. Abidin, H. Andreas, I. Gumilar, D. Sarsito, R. Hanifa, Rino, H. Harjono, T. Kato, F. Kimata, and Y. Fukuda (2012). Slip Rate Estimation of the Lembang Fault West Java from Geodetic Observation. *JDR* **7(1)**, 12–18.
32. Molnar, S., J. F. Cassidy, K. B. Olsen, S. E. Dosso, and J. He (2014). Earthquake ground motion and 3D Georgia basin amplification in SW British Columbia: Deep Juan de Fuca plate scenario earthquakes. *Bull. Seism. Soc. Am.* **104**, 301–320.
33. Molnar, S., J. F. Cassidy, K. B. Olsen, S. E. Dosso, and J. He (2014b). Earthquake ground motion and 3D Georgia basin amplification in SW British Columbia: Shallow blind-thrust scenario earthquakes. *Bull. Seism. Soc. Am.* **104**, 321–335.
34. Musson, R. M. W. (2012). A provisional catalogue of historical earthquakes in Indonesia. *British Geological Survey*
35. Nata, T. P. and B. Witsen (100). A Relation of the Bad Condition of the Mountains about the Tungarouse and Batavian Rivers, Having Their Source from Thence, Occasioned by the Earthquake between the 4th and 5th of January, 1699. Drawn up from the Account Given by the Tommagon Porbo Nata, (Who Hath Been There) and Sent to the Burgermaster Witsen, Who Communicated It to the R. Society, of Which He is a Member. *Philosophical Transactions* **22(260-276)**, 595–598.
36. Ng, A. H.-M., L. Ge, X. Li, H. Z. Abidin, H. Andreas, and K. Zhang. (2012). Mapping land subsidence in Jakarta, Indonesia using persistent scatterer interferometry (PSI) technique with ALOS PALSAR. *Int. J. Appl. Earth Obs. and Geoinfo.* **18**, 232–242.
37. Nguyen, N., J. Griffin, A. Cipta, and P. Cummins (2015). Indonesia's Historical Earthquakes Modelled examples for improving the national hazard map. *Geoscience Australia* Record **2015/23**, Canberra
38. Pilz, M., S. Parolai, M. Stupazzini, R. Paoluci, and J. Zschau (2011). Modelling basin effects on earthquake ground motion in the Santiago de Chile basin by a spectral element code. *Geophys. J. Int.* **187(2)**, 929–945.
39. Pusat Litbang Perumahan dan Pemukiman PU (2011). $http://puskim.pu.go.id/Aplikasi/desain_spektra_indonesia_2011/$, accessed on November 20, 2017.
40. Pusat Studi Gempa Nasional (National Center for Earthquake Studies) (2017). *Peta Sumber dan Bahaya Gempa Indoensia Tahun 2017*, Pusat Litbang Perumahan dan Pemukiman PU, Bandung, Indonesia.
41. Putra, S. D. H., Suryantini, and W. Srigutomo (2016). Thermal modeling and heat flow density interpretation of the onshore Northwest Java Basin, Indonesia. *Geothermal Energy* 4(12)
42. Rial, J. A., N. G. Saltzman and L. Hui (1992). Earthquake-induced resonance in Sedimentary Basin. *American Scientist* **80(6)**, 566–57.
43. Ridwan, M. (2016). Development of an engineering bedrock map beneath Jakarta based on microtremor array measurements. Study of Ground Subsurface in Jakarta by Using Microtremor Array Method: Identifi- cation of Engineering Bedrock Depth and Site Class. *Dissertation at Institut Teknologi Bandung*, Bandung, Indonesia.
44. Shoji, Y., K. Tanii, and M. Kamiyama (2004). The Duration and Amplitude Characteristics of Earthquake Ground Motions with Emphasis on Local Site Efects. Conference Paper No. 436. *the* 13_{th}*WCEE* Vancouver, B.C., Canada.

Peer-reviewed version available at *Geosciences* **2018**, *8*, 128; doi:10.3390/geosciences8040128

45. Simandjuntak, T. O. and A. J. Barber (1996). Contrasting tectonic styles in the Neogene orogenic belts of Indonesia. *Geol. Soc., London, Special Publications* 106(1), 185–201
46. Simons, W. J. F. , A. Socquet, C. Vigny, B. A. C. Ambrosius, S. H. Abu, C. Promthong, C. Subarya, D. A. Sarsito, S. Matheussen, P. Morgan, and W. Spakman (1997). A decade of GPS in Southeast Asia: resolving Sundaland motion and boundaries. *J. Geophys. Res.* **112(B6)**, n/a–n/a.
47. Supartoyo, I. A. Sadisun, E. Suparka, and Abdullah (1997). Cimandiri Fault Activity at Sukabumi Area, West Java, Indonesia (Based on Morphometry Analysis). *Proceedings: ISEGA I*, 76–83.
48. UBC (2003). *International Conference of Building Officials. Uniform Building Code*, Willier, California
49. Wang, W. J., K. F. Ma, F. Mothereau, and D. Eberhart-Phillips (2009). Three-dimensional Qp- and Qs-tomography beneath Taiwan orogenic belt: implications for tectonic and thermal structure *Geophys. J. Int.* **180(2)**, 891–910
50. Wiegel, R. L. (1970) *Earthquake Engineering* 518 pp, Prentice-Hall, Englewood Cliffs, N. J., 22, 209.
51. Zhao, Z., Z. Zhao and J. Xu (2010). Interference between seismic body wave and secondary surface wave resulting in the peak collapse ratios of buildings. *J. Appl. Geophysics* **72(1)**, 1–9.

Sample Availability: Samples of the compounds ...... are available from the authors.